

Full-scale analysis of deformation and stress distribution for constrained composite bearing elements under compressive yielding conditions

P. Samyn^{a,*}, L. Van Schepdael^b, J.S. Leendertz^c, A. Gerber^d, W. Van Paepegem^a, J. Degrieck^a, P. De Baets^a

^a Ghent University, Laboratory Soete, Department of Mechanical Construction and Production, St. Pietersnieuwstraat 41, B-9000 Gent, Belgium

^b SOLICO B.V., Solutions in Composites, Everdenberg 97, NL-4902 TT Oosterhout, The Netherlands

^c Ministry of Transport, Public Works and Water Management, Directorate-General, Herman Gorterhove 4, NL-2700 AB Zoetermeer, The Netherlands

^d University of Stuttgart, Staatliche Materialprüfungsanstalt, G-70550 Stuttgart (Vaihingen), Germany

Received 18 January 2006; accepted 4 September 2006

Available online 31 October 2006

Abstract

Five hundred composite pads with nominal diameter 250 mm and thickness 40 mm are used as bearing elements in a redesigned ball-joint, maximum loaded at 150 MPa under normal working conditions. Above their yield strength, softening of the top surface is favourable for smooth sliding while the dimensional stability should be controlled by reinforcements. Pads are therefore incorporated into separate steel holes and the top surface is additionally stabilised by a carbon fibre/epoxy ring. A “local” study on a single bearing element by full-scale static deformation and creep tests with an evaluation of stresses and deformation by finite element simulations is presented in this paper. Yielding was observed above 50 MPa, with consequent increase in stiffness due to the constraining action of the steel sample holder. Long time creep at 60–150 MPa is stabilised after total constraint, with the composite pad under hydrostatic stress conditions. Finite element modelling is used for short-time and long-time deformation as a function of different pad geometries (thickness, diameter and fixation methods) and Young’s moduli. Mainly deformation of a polymer lip at the top surface and extrusion near circumferential polymer grooves, containing a rubber ring for axial fixation, is studied. The contact between a convex counterface and the polymer top surface is modelled, and full contact occurs when loaded above 50 MPa, showing a complex interaction between immediate elastic deformation, long-term creep and variable contact geometry as reflected in the stress–strain characteristics. Under high loads, there is a transition in bulk modulus implied by the test geometry. Finally, the strength of the composite pads and the steel constraining walls is verified.

© 2006 Elsevier Ltd. All rights reserved.

Keywords: Full-scale; Finite elements; Composite design; Creep; Strength

1. Introduction

The deformation mechanisms and visco-elastic modelling of composite materials have received much interest due to the increased use in a broad range of civil engineering constructions. Particularly in critical load bearing applications, soft materials (polyamides, polyacetals, poly-

ethylenes, etc.) or fibre-reinforced polymer matrix composites are replacing metallic parts because of the self-lubricating ability. They are expected to exhibit the same (or better) reliability and predictability as metallic components, requiring an adequate lifetime analysis in parallel to the design process. A major problem in this respect is the dimensional stability of bearing elements during loading and unloading. As composite parts are often designed as functional parts, high deformation can cause failure of the structure due to loss of clearance. The first step in a

* Corresponding author. Tel.: +32 9 264 33 08; fax: +32 9 264 32 95.
E-mail address: pieter.samyn@UGent.be (P. Samyn).

design process is often based on experimental experience, as the mathematical analysis of visco-elasticity is rather complex due to non-linearity and strain rate dependent material properties, non-linear unloading characteristics, the effect of a hydrostatic pressure on yielding, the influence of cyclic creep and significant recovery at zero stress. An additional problem is the analysis of an effective structure that limits creep and deformation under yielding conditions. However, for a correct implementation and verification of the capacity of the entire structure, a comprehensive model of the local polymer composite parts is needed, that represents the effects of elastic–plastic, time-dependent and permanent deformation.

In recent years, a number of constitutive equations has been described for the time-dependent mechanical behaviour of polymeric materials: Boyce et al. [1], Krempl and Bordonaro [2], Hasan and Boyce [3], Bardenhagen et al. [4], Takashi et al. [5], Yang and Chen [6], Khan and Zhang [7], Van Dommelen et al. [8]. A model based on the interaction of macromolecular networks was presented by Bergström and Boyce [9]. The total strain is assumed to be the sum of an elastic strain, subjected to the Hooke's law, and a viscoplastic strain, derived from the kinetic hardening creep theory of Malinin and Khadjinsky [10]. The latter is assumed to be incompressible and independent on the hydrostatic stress. Particularly for overstress situations, Krempl and Ho [11] developed an "Overstress model for solid polymer deformation behaviour applied to Nylon 66" and Colak [12] performed numerical simulations in overstress on polyphenylene-oxide under monotonic loading and unloading at various strain rates, multiple creep and recovery. Since creep behaviour was found to be profoundly influenced by the level of stress, tests were performed at different stress levels above and below yield stress and the original overstress model was modified for reproduction of the non-linear rate-dependent behaviour. The theory consists of two tensor variables and two scalar variables:

- The equilibrium stress is the path-dependent stress that can be sustained at rest after prior inelastic deformation; it is related to the defect structure of the material.
- The kinematic stress is the repository for modelling the Bauschinger effect and sets the tangent modulus at the maximum strain of interest.
- The isotropic stress is a rate-dependent stress responsible for hardening or softening.
- The drag stress is a time-dependent factor.

For practical engineering, the importance of each factor above depends strongly on a multiaxial stress condition introduced in certain applications. General models often do not take into account specific contact geometries or boundary conditions implied by the surrounding construction, although they possibly induce specific hydrostatic stresses. Input values as Young's moduli should therefore often be replaced into a 'bulk modulus' in order to model

the exact state of stress and deformation of the polymer component. As the latter is influenced by the test layout and is scarcely reported in literature, it should be determined experimentally from a test set-up that simulates the real working environment as closely as possible. One particular case study is therefore presented in this paper, concerning the redesign of a highly loaded ball-joint in the Maeslant storm surge barrier near Rotterdam (NL) where polymer composite pads were introduced as sliding material. Experimental full-scale test results on friction and wear properties of the bearing elements were previously reported by Samyn et al. [13], while validation tests on compressive strength were also evaluated by Samyn et al. [14]. Based on experimental results, local deformation and creep will be analysed by finite element modelling of the reinforced bearing elements and strength verification of the constraining walls. Attention should be specifically given to the effect of a convex counterface, the dimensional stability of the reinforcing carbon ring and the stability of an appropriate fixation method. This study was done in an international test program at Ghent University (Laboratory Soete), Solico (solutions in composites) and Stuttgart University (Materialprüfungsanstalt), while the final concept was implemented and proven on-the-field by the "Nederlandse Rijkswaterstaat".

2. Geometrical bearing situation

The Maeslant storm surge barrier consists of two walls that are swung into the Nieuwe Waterweg river during a storm. The rotation is ensured by a ball-joint in the abutments of the structure. It has a faceted ball (convex) surface with diameter 10 m made of cast steel, sliding into concave steel supports. As both surfaces were originally covered with a sliding spray of molybdenum disulfide (MoS_2) and polytetrafluoroethylene (PTFE), severe wear was observed and a new bearing concept should be implemented. Five hundred polymer pads are placed into machined holes on the concave steel parts, each with diameter 250 mm. As the top surface of these elements is positioned at 8 mm above the steel surface, the polymer parts take the full load and have to resist the shear forces during sliding. From finite element calculations on the entire construction, the maximum load on one single bearing element is 150 MPa.

The characteristics and implications of the modified sliding system on the *global* surge barrier construction are beyond the scope of present report, and are detailed elsewhere by Leendertz et al. [15]. Presently, only the *local* behaviour of a single polymer bearing element constrained in a machined hole will be studied and modelled in contact with a ball steel counterface. An important issue is the local elastic deformation caused by geometrical imperfections of the convex counterface. For stable functioning of the ball-joint, the normal deformation of the polymer sliding surface should be limited to 1 mm as it causes an additional stress in the polymer bearing element: e.g. for an average

contact pressure of 90 MPa, an implied additional deformation of 1 mm results in a total stress of 150 MPa acting on a single bearing element. Therefore, the local deformation on a polymer bearing element should be modelled by its stress–strain behaviour that is characteristic for short-time loading (i.e. immediate application of the load without considering creep). During further modelling of long-term loading, creep possibly causes a redistribution of the contact stresses and stabilises the local deformation. In this respect, the reinforcing action of the constraining holes should be verified by considering the effective stiffness of a bearing element. It should be experimentally verified that the resulting contact pressures not exceed the loading capacity of the polymer pads.

3. Experimental

3.1. Test materials for composite bearing elements

As depicted in Fig. 1, two materials are considered for evaluation of the pad stiffness and deformation at the top layer: (a) polyester/polyester composite pads with PTFE additives dispersed in the top layer for beneficial sliding properties and (b) a hybrid Ultra-high molecular weight polyethylene (UHMWPE) polymer pad. Thermal and mechanical properties of both materials used as bearing elements, are listed in Table 1.

The polyester/polyester pads consist of 90° polyester wovens that are impregnated with a thermosetting polyester resin. In the top surface (5 mm) PTFE solid lubricant is homogeneously dispersed into the matrix. As it is a relatively new material for marine applications under extremely high loads, little relevant literature about its performance is available. It is mainly used as cylindrical bearings under low loads and high sliding velocities. The independent elastic properties of the orthotropic material were determined in the frame of this project from a preliminary study on small-scale tensile tests, compression tests and short beam shear tests as

follows [16]: $E_{11} = 2.36$ GPa, $E_{22} = 2.19$ GPa, $\nu_{12} = 0.30$ to 0.35 , $\nu_{23} = 0.45$ – 0.50 (experimental) and $G_{13} = G_{23} = 700$ MPa (calculated). The deformation stability was mainly determined by the lubricated top layer as the matrix is locally weakened. From manufacturer's catalogues [17] a pure elastic deformation of 10% is expected when axially loaded (perpendicular to the woven structure) below 120 MPa, characterised by a nearly linear stress–strain relationship. No significant permanent deformation is reported for the polyester/polyester bulk composite after recovery. Under constrained conditions, a maximum static loadability of 345 MPa is expected. It has a density of 1.25 g/cm³ and is thermally stable between -40 °C and 130 °C in dry environment.

The hybrid UHMWPE pads consist of non-regenerated GUR 4120 [18] that is compression moulded with intrinsic viscosity 2400 ml/g, density 0.93 g/cm³, average molecular weight of $5 \cdot 10^6$ g/mol. It has a melting point of 130 °C and Vicat softening point of 80 °C with 48–56% crystalline content and hardness Shore D 60. Tensile Young's modulus is 720 MPa, elongation at yield 20% and elongation at fracture >50%. Creep properties according to ISO 899 standards are obtained under tensile stress, although serving as a good approximation for the values to be expected under compressive stress. Strictly speaking, separate values should be determined for each type of stress. Only under low deformation the variation between characteristic values is negligible, so that the time-dependent compression of a component may be calculated with sufficient accuracy using the flexural creep modulus. Present application at 150 MPa however largely exceeds the polymer yield strength (20–25 MPa) and needs additional analysis. A reinforcing composite ring is made of unidirectional carbon fibre Toray T700 12K (1.8 g/cm³) and epoxy resin (1.09 g/cm³) that is hoop wound and machined into separate rings. It has fibre percentages between 58% and 63% and a porosity content <2.5%. The curing times and temperatures were 16 h at room temperature, 8–10 h at 60 °C and 8–10 h at 120 °C (15 °C/h).

Dimensions and tolerances of the bearing elements are determined from an experimental evaluation of stable deformation [14]: in the final layout, both bearing element types have a nominal diameter of 249.50 mm (0.50 mm clearance with holder for proper assembly) and thickness 40 mm. The reinforcing carbon fibre/epoxy ring of hybrid UHMWPE pads has a nominal outer diameter of 249.00 mm with appro-

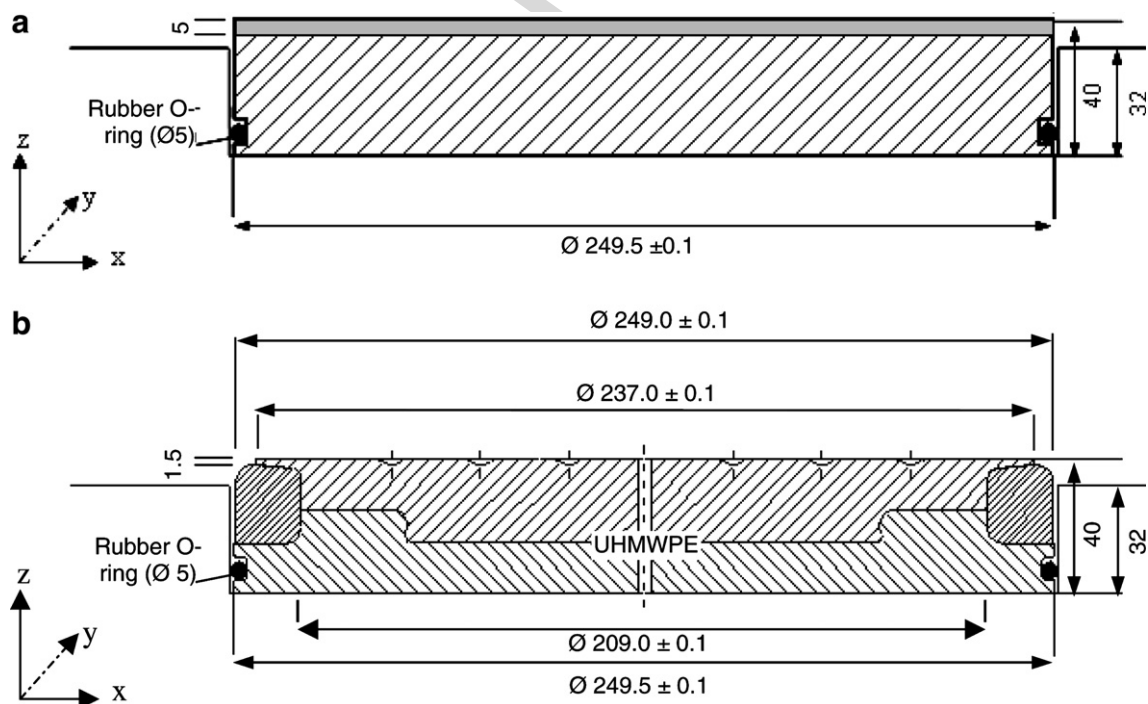


Fig. 1. Full-scale bearing elements, constrained into a steel sample holder with diameter 250 mm, (a) polyester/polyester pad with PTFE lubricated top-layer (5 mm), (b) hybrid UHMWPE pad with carbon fibre/epoxy ring.

Table 1
Mechanical and thermal properties of polyester/polyester and hybrid UHMWPE pads

	Density (g/cm ³)	Young's modulus (MPa)	Compressive strength (MPa)	Hardness	Thermal properties (°C)
Polyester/polyester	1.25	3200	345 (perpendicular fibres) 95 (parallel fibre)	100 Rockwell M	−40 (min working temperature) 130 (max working temperature)
UHMWPE	0.93	720	>17 (yield stress)	60 Shore D	42 (heat deflection 1.8 MPa) 80 (Vicat softening) 130 (Melting point)

priate fillets. It should however be protected against direct contact with the steel counterface, as it leads to unacceptable counterface wear during sliding. A polymer lip has therefore been designed with diameter 237 mm and thickness 1.5 mm. Different axial fixation methods will be further evaluated with a rubber O-ring (diameter 5.6 mm) as best option.

3.2. Full-scale test equipment

Compressive loading tests on full-scale bearing elements with variable diameter are done at Ghent University on a hydraulic vertical loading frame with maximum capacity of 10,000 kN. Specimens are positioned in a sample holder with fixed diameter 250.00 mm and depth 32 mm, according to the boundary conditions in the practical bearing application (Fig. 2a). A ball counterface with radius 5000 mm and Zn-phosphate primer coating for protection against corrosion is used in contact with the pad top surface. The sample holder is horizontally centred on a table under the hydraulic press and loaded by a vertical jack pushing the holder and its pad against the fixed upper frame plate. The vertical displacement between the upper frame plate and the table is measured by linear transducer sensors (LVDT). The load is applied at a constant stress rate (30 MPa/min) to a maximum of 150 MPa and then unloaded at the same rate. Intermediate contact pressures of 30, 60, 90 and 120 MPa are kept constant for 2 h during stepwise loading, corresponding to a normal load of respectively 1472, 2945, 4417, 5890 and 7263 kN (72.6% of the load cell capacity). Long-time creep is afterwards measured during a 24 h test. A second loading step was performed from 0 to 180 MPa maximum load. The latter overload test is important in multiple loading of the ball-joint. Each test was done at room temperature and was repeated three times, showing good reproducibility (2.4% standard deviation on maximum indentation at 150 MPa [14]).

Static loading tests were also done at Stuttgart University on small-scale bearing elements, giving insight in the effect of pad and counterface geometries, lubrication and constraining action of the carbon fibre/epoxy ring. An UHMWPE pad without carbon fibre/epoxy ring (diameter 149.50 mm and thickness 17 mm) is mounted in a steel sample holder (diameter 150.00 mm and depth 13 mm) and loaded under 10, 30 and 50 MPa contact pressures against a flat counterface (Fig. 2b). The contact interface is either dry or lubricated with a high-contact-pressure type of grease.

4. Test results

4.1. Stress vs strain characteristics in full-scale compression tests

The engineering stress–strain curves for deformation of full-scale constrained bearing elements are shown in Fig. 3a (polyester/polyester pads with diameter 248.00 and 249.50 mm) and Fig. 3b (hybrid UHMWPE pads with diameters of 249.37, 249.50 and 249.55 mm). The engineering stress under compressive load was calculated as $\sigma_c = F/A_0$ and the engineering strain corresponds to $\varepsilon = \Delta h/40$ with Δh the measured axial compression. The true strain

under compressive loading is calculated as $e = -\ln(1 - \Delta h/40)$ and is plotted in Fig. 3c and d for polyester/polyester or hybrid UHMWPE pads, respectively.

In case of hybrid UHMWPE pads, the true stress–strain behaviour is compared to test data of Kurtz et al. [19], who performed small-scale compressive tests on the yielding, plastic flow and fracture behaviour of UHMWPE under low contact stresses (<30 MPa). He used unreinforced cylindrical UHMWPE samples with 10 mm diameter and 15 mm length. One conclusion of his work was that the true stress–strain curve is identical under both tensile and compressive stress up to a true strain $e = 0.12$. For present constrained hybrid UHMWPE pads, a low stiffness is shown during initial contact with the convex counterface, as a 10 kN normal load results in 0.70 mm axial compression ($\varepsilon = 1.75$ or $e = 0.018$). The initial point contact in the centre of the polymer pad causes local stress concentrations that are not dimensionally stabilised by the carbon fibre/epoxy ring due to the initial clearance between the bulk UHMWPE and its ring. Compared to the true stress–strain curves (Fig. 3d), this region $e < 0.02$ corresponds to the elastic zone of UHMWPE with a linear stress–strain relation. For higher strains, the central polymer element is fully constrained by its carbon fibre/epoxy ring and for $e = 0.02$ – 0.04 , the constrained pad shows a linear increase in strain with increasing stress. The true strain $e = 0.04$ corresponds to the onset of plastic deformation at a yield strength of 21 MPa according to Kurtz et al. [19], and a progressive increase in stiffness is measured due to the constraining action of the steel walls of the sample holder. A non-linear relation is initially observed through progressive indentation of the convex counterface below 50 MPa. For deformation at higher loads, the stiffness attains 3879 kN/mm under 120 MPa towards 4910 kN/mm under 150 MPa (27% increase), which is the region of interest for present design. It is however observed that the deformation at low loads is more complex due to the additive phenomena of counterface geometry, counterface friction, reinforcing carbon ring and reinforcing steel walls. The deformation above yield strength is however stabilised with a high stiffness induced by the reinforcing system and flexibility of the polymer element.

For polyester/polyester pads with free top surface, a different deformation path is recorded, mainly under low loads. Due to the higher intrinsic modulus and strength, the deformation during initial contact with the convex counterface is lower compared to UHMWPE, with linear

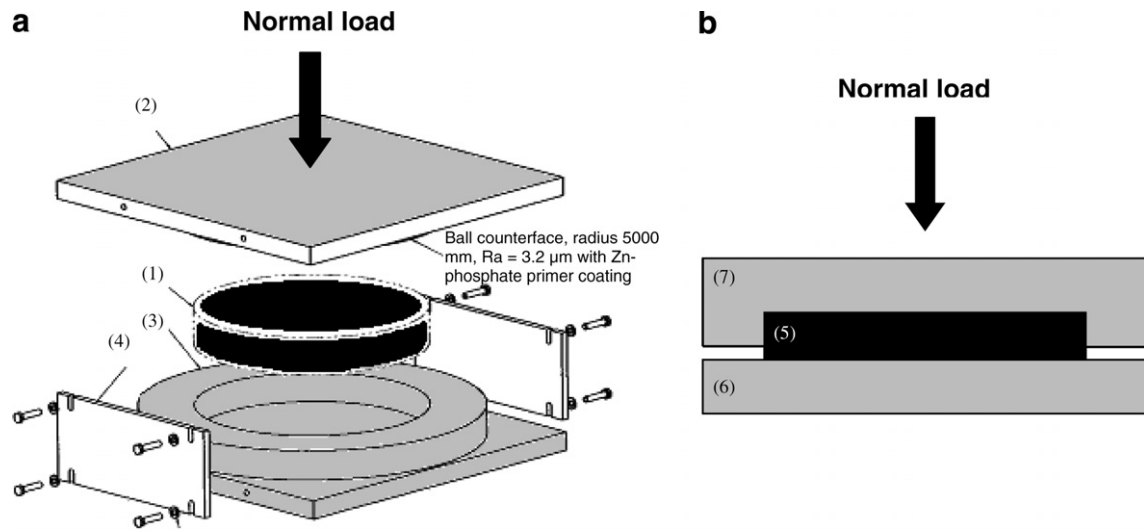


Fig. 2. Test set-up for compressive loading of constrained bearing elements, (a) full-scale test equipment at Ghent University, (b) small-scale test equipment at Stuttgart University (1) full-scale pad (\varnothing 249.50 mm), (2) counterface with convex radius $R = 5000$ mm, $R_a = 3.2 \mu\text{m}$ with Zn-phosphate primer coating, (3) steel sample holder (\varnothing 250.00 mm), (4) clamps for positioning, (5) small-scale pad (\varnothing 149.50 mm), (6) flat counterface, (7) steel sample holder (\varnothing 150.00 mm).

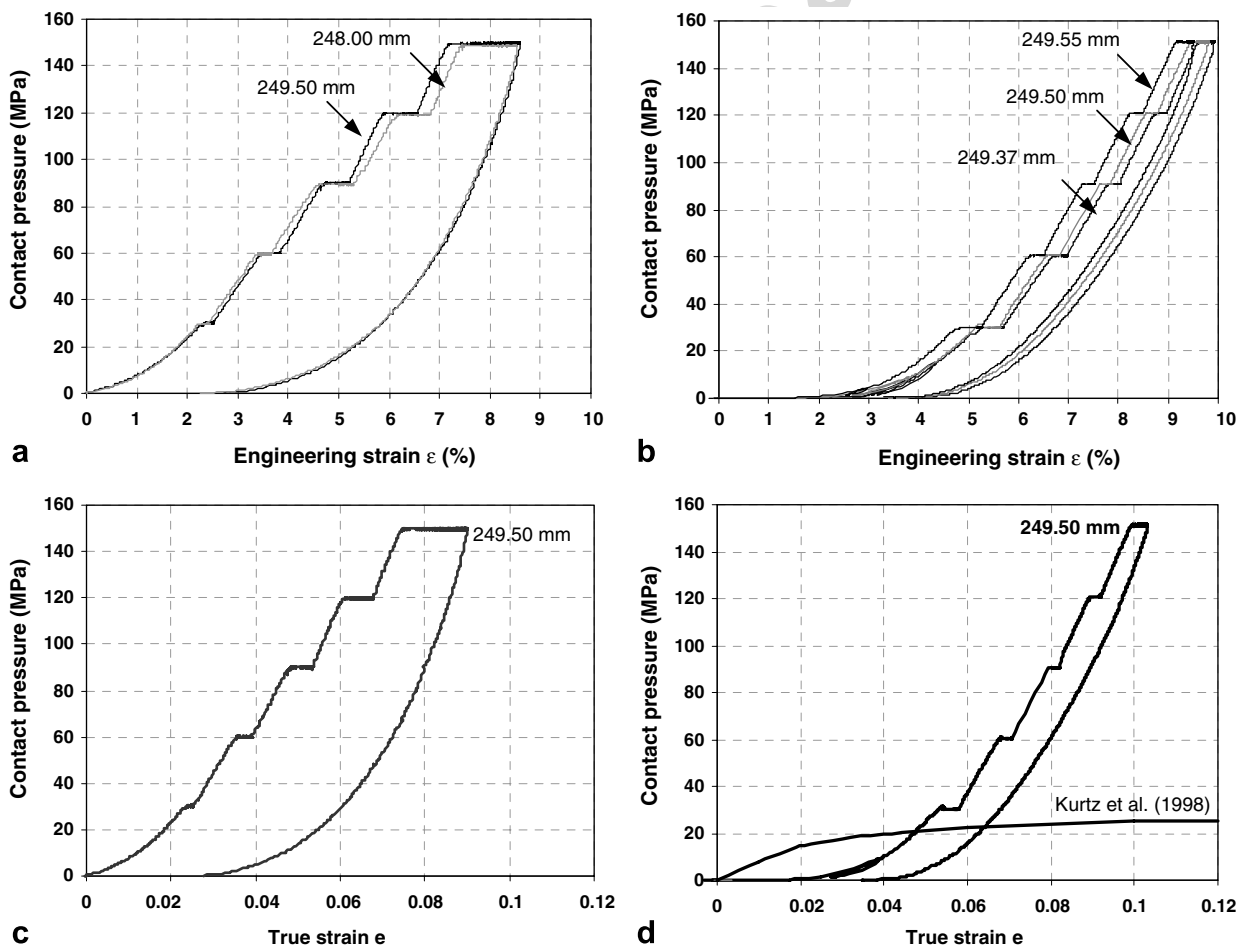


Fig. 3. Stress–strain characteristics for constrained bearing elements with different effective diameters, (a) engineering strain for polyester/polyester, (b) engineering strain for hybrid UHMWPE, (c) true strain for polyester/polyester, (d) true strain for hybrid UHMWPE.

stress–strain for $e < 0.01$ or normal contact pressures below 10 MPa. The dimensional stability of the bulk polymer is presently not influenced by a reinforcing carbon fibre/

epoxy ring and only the clearance between the bulk polymer and the steel sample holder is important: for higher normal loads or strains $e > 0.01$, the clearance has disap-

peared through elastic deformation and in agreement with the hybrid UHMWPE pads, there is noticed a gradual increase in stiffness to 4837 kN/mm under 120 MPa or 5220 kN/mm under 150 MPa (7% increase). The increment in stiffness for polyester/polyester pads is lower than for hybrid UHMWPE pads as important deformation was presently observed at the free top surface. The influence of clearance and constraint is evaluated by loading a composite pad with initial diameter 249.00 mm either constrained in a sample holder (diameter 250.00 mm) or on a free bottom plate, recording both the axial compression and radial expansion (Fig. 4). The total axial deformation of 9.5 mm is evidently higher for non-constrained pads with high radial creep (17.3 mm) when loaded above 50 MPa. However, a detail of the deformation at low loads shows an identical linear stress–strain relation for constrained and non-constrained pads only for small strains $e < 0.01$ (0.20 mm axial indentation). The increase in stiffness for constrained pads for $e > 0.01$ is then attributed to fitting of the rubber O-ring at the bottom of the constrained pad as the radial deformation is only 0.07 mm. Complete radial fitting of the entire pad is attained when

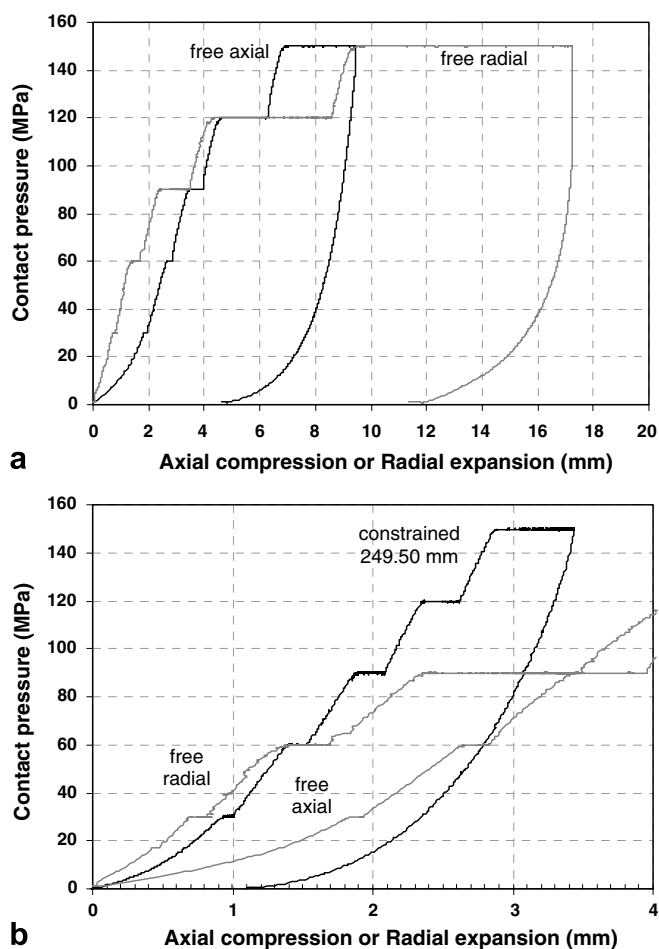


Fig. 4. Stress–strain characteristics for free polyester/polyester pads, (a) axial compression and radial expansion, (b) detail of low load region comparing free and constrained bearing elements.

the radial expansion is 0.50 mm, resulting in a further increase in stiffness for contact pressures above 20 MPa.

The effect of clearances on the deformation of a hybrid UHMWPE pad was more extensively discussed in Ref. [14]. The total deformation at 150 MPa for pads with small diameter is higher compared to pads with large diameter due to differences in constraining action of the steel sample holder, while the final stiffness (kN/mm) does not vary significantly in correspondence to previous deformation mechanism.

Both polyester/polyester and hybrid UHMWPE pads exhibit a nonlinear unloading curve, according to data for polymers as polytetrafluoroethylene [7], polyetheretherketone and Nylon 66 [2] or polyphenylene oxide after loading above its yield strength. Although this deformation was successfully modelled by Colak [12] with an overstress model, present stress–strain curve is also influenced by contact with a convex counterface and reinforcing action of the carbon fibre/epoxy ring or sample holder. During a second loading step, the stress–strain curves from Fig. 5 are different compared to the first loading step, as the initial clearance presently does not have importance. The stiffness has increased significantly compared to the first loading step, and the constraining action allows for low axial compression of hybrid UHMWPE pads. For polyester/polyester pads, this effect was less significant as the weak lubricated top layer fractured.

4.2. Creep in full-scale compression tests

Creep measurements during 24 h loading are given in Fig. 6a for a polyester/polyester pad and in Fig. 6b for a hybrid UHMWPE pad, both with nominal diameter 249.50 mm and constrained. For polyester/polyester pads, the total creep is between 0.10 and 0.55 mm with two

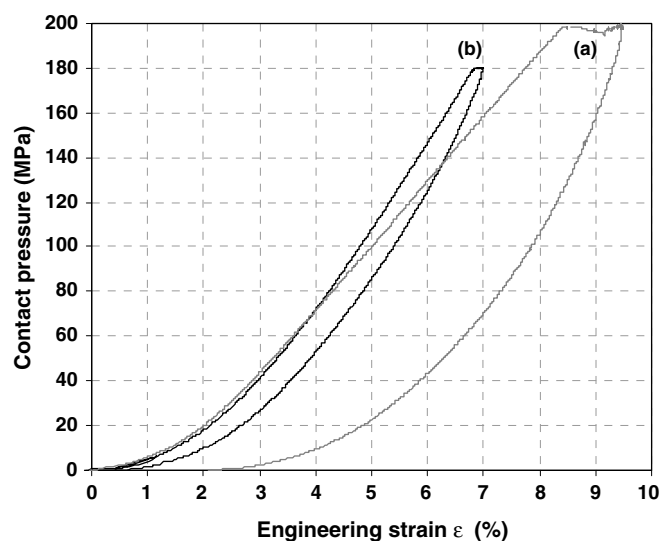


Fig. 5. Stress–strain characteristic for a second loading step (overload verification to 180 MPa or 200 MPa) on (a) polyester/polyester pads, (b) hybrid UHMWPE pads.

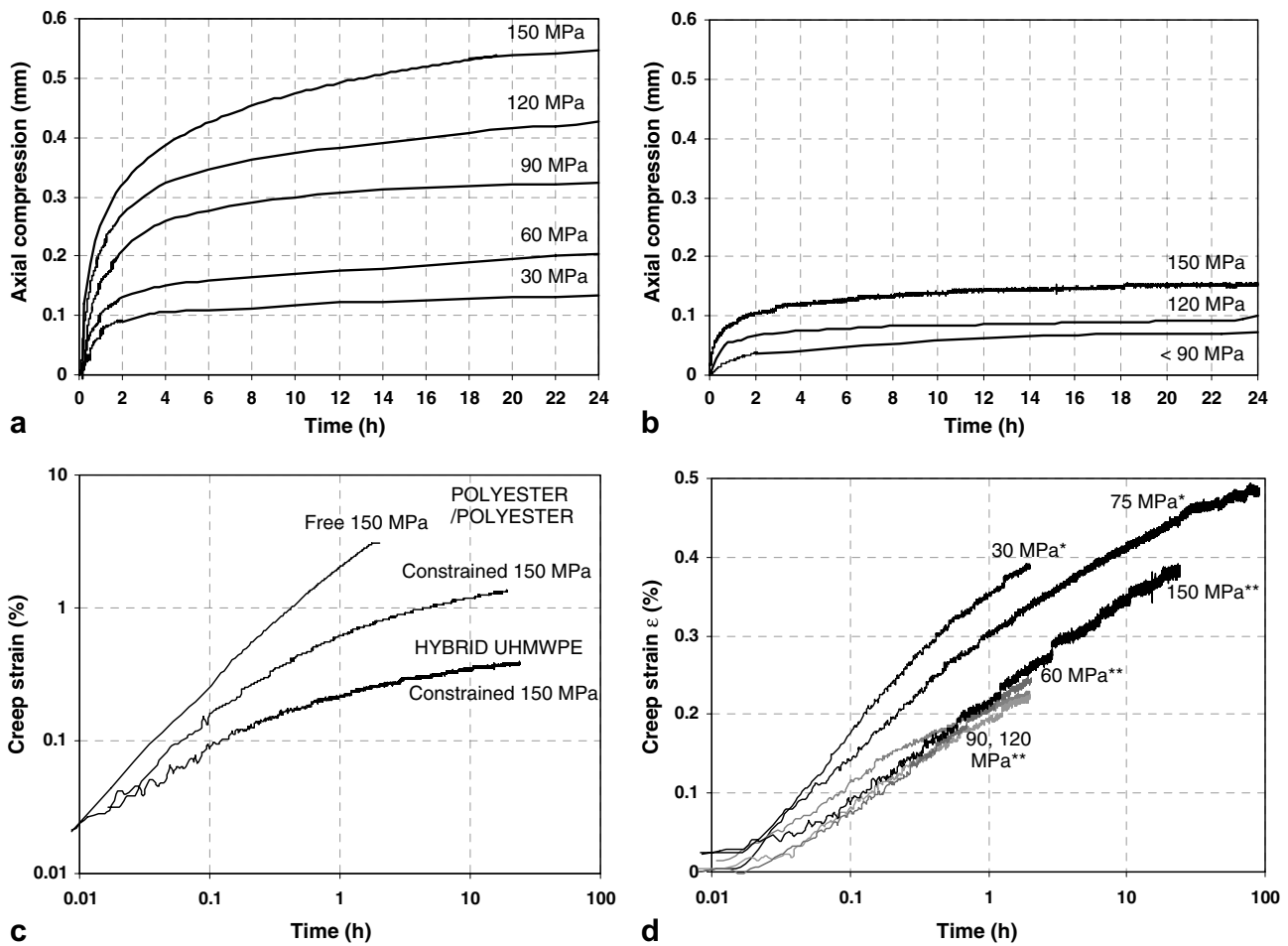


Fig. 6. Creep deformation of constrained bearing elements, (a, c) polyester/polyester pads, (b, d) hybrid UHMWPE pads for * single loading step or ** stepwise loading.

regimes: a linear increase in axial deformation occurs for the 30 and 60 MPa loads, while there is a non-linear creep for 90–150 MPa loading. In the latter cases, the axial compression linearly increases to 0.15 mm axial displacement with subsequent decreasing slopes at higher loading times. According to Fig. 4b, it is verified that the 0.15 mm axial compression corresponds to 0.25 mm radial expansion, as such that the initial clearance of 0.50 mm between pad diameter and sample holder has disappeared. The high creep was however unallowable in relation to practical design. Creep for hybrid UHMWPE pads is much lower, attributed to stabilisation of the top surface by the carbon fibre/epoxy ring.

Creep deformation is mostly described by the well-known power law verified by e.g. Scott and Zureick [20] for time-dependent deformation of thermoplastics. The simplest form of the power law is written in Formula (1),

$$\varepsilon(t) = \varepsilon_0 + mt^n \quad (1)$$

where $\varepsilon(t)$ is the total time-dependent creep strain, ε_0 is the stress-dependent and temperature-dependent initial elastic strain, t is the time after loading and the parameters m and n empirical constants to be determined from a double

logarithmic plot. In Fig. 6c, creep of a free and constrained polyester/polyester pad is compared. While it is observed from the linear relation in a double logarithmic plot that free compressive deformation can be described by previous equation, the constraint of a steel sample holder causes lower deformation. This is adequately demonstrated on a plot with logarithmic time and linear creep strain (Fig. 6d), indicating linear deformation of constrained hybrid UHMWPE pads under different contact pressures, according to Formula (2):

$$\varepsilon(t) = \varepsilon_0 + m \log t \quad (2)$$

Different loading histories are compared in Fig. 6d for a two-hours creep test, with either (i) a single loading step at 30 MPa, (ii) stepwise loading at 30, 60, 90, 120 and 150 MPa. One verification test was done for 168 h loading at 75 MPa. It is observed that the creep strain rate under steady-state conditions is nearly independent of the normal load. The deformation is similar for stepwise 90–150 MPa loading, even after multiple loading steps. This is an important issue in respect to the practical implementation and life-time use of the bearing elements in the ball-joint. Variable deformation is however concentrated within the first

loading period under low loads. High initial deformation is observed under 30 MPa as visco-elastic deformation is initially attributed to elimination of the clearance; the creep is further controlled by total constraint after 45 min loading. Under 75 MPa this initial deformation step is somewhat reduced as the immediate elastic deformation is higher when load is applied; steady-state creep is attained more frequently. For a second loading step, this transition period has almost disappeared under 60 MPa (a small transition period remains due to elastic recovery at unloading) and has completely disappeared at 90–150 MPa.

4.3. Recovery and permanent deformation

The dimensional recovery and permanent deformation after 24 h creep at 150 MPa is given in Table 2 for various

bearing elements, both with constrained or free radial expansion, resulting in 0.70 mm permanent axial compression of hybrid UHMWPE pads and 1.20 mm for polyester/polyester pads. Test specimens are photographed in Fig. 7. Although it was observed in Fig. 3 that the total axial compression is nearly identical for constrained polyester/polyester and hybrid UHMWPE pads, the integrated area under the stress–strain curve is significantly larger for polyester/polyester pads, representing higher deformation hysteresis. In combination with the intrinsic elastic properties, this resulted in a high permanent axial compression of polyester/polyester pads, mainly concentrated in shear fracture of the weak PTFE-lubricated top surface (Fig. 7a). For free polyester/polyester pads, high radial expansion of the bulk at mid-height (‘bulge-like’) was observed, as also experienced on small-scale

Table 2
Recovery and permanent deformation of bearing elements after 150 MPa load

		Recovery (mm)		Permanent deformation (mm)
		Immediate unloading	24 h stress free	
<i>UHMWPE with carbon fibre/epoxy ring</i>				
Constrained	Axial compression	2.60	0.63	0.70–0.74 ^a
	Radial expansion	–	–	0.12–0.23 ^a
<i>Polyester/polyester</i>				
Constrained	Axial compression	2.35	0.37	0.76–1.20 ^a
	Radial expansion	–	–	0.87–1.88 ^a
Free	Axial compression	4.86	1.10	2.38
	Radial expansion	5.92	3.16	2.95

^a Depending on clearance.

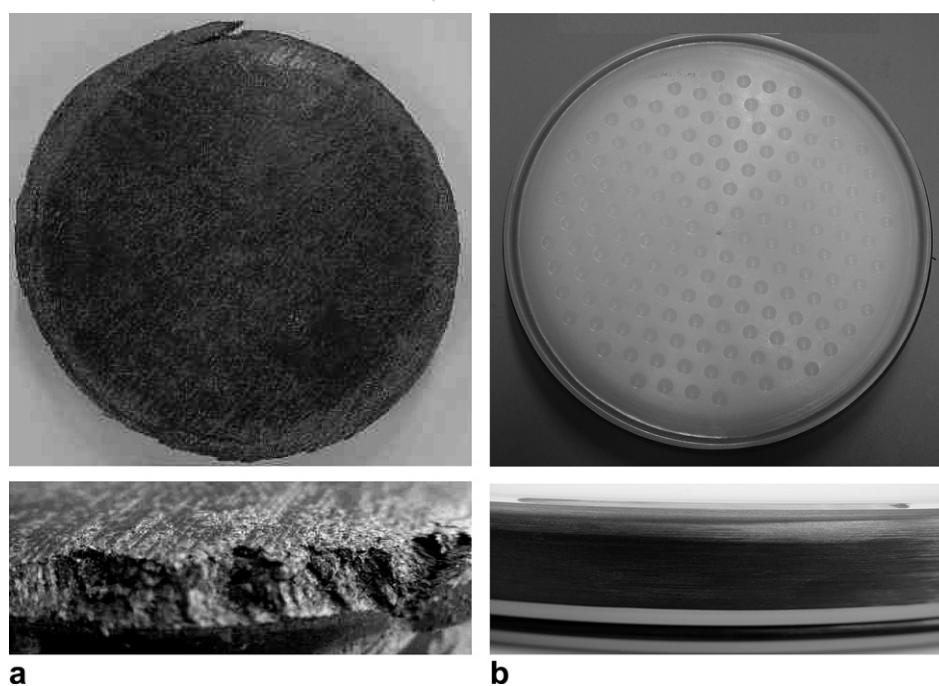


Fig. 7. Permanent deformation of bearing elements (diameter 249.50 mm) after 150 MPa compressive load in top and side view, (a) polyester/polyester pad, (b) hybrid UHMWPE pad.

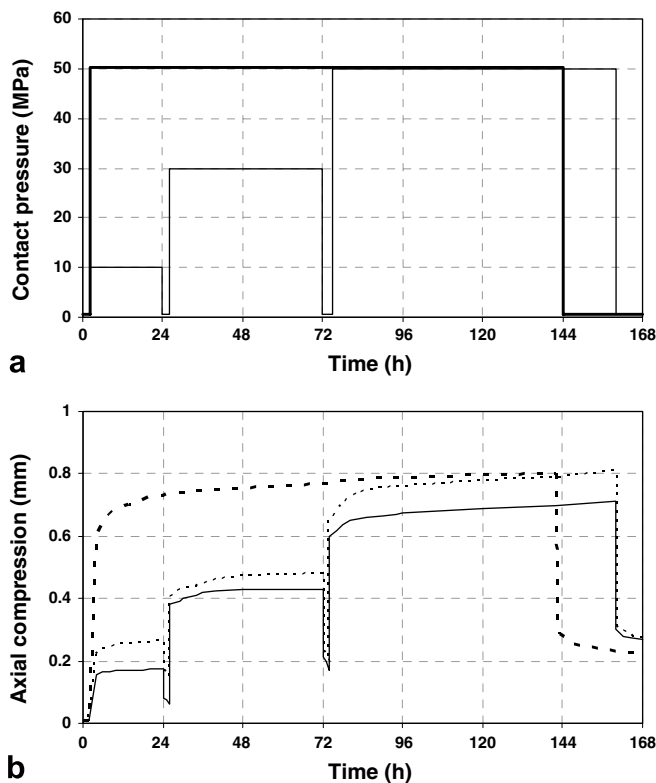


Fig. 8. Creep of small-scale UHMWPE pads without carbon fibre/epoxy ring and flat counterface under dry (full line) and lubricated conditions (dotted lines) measured at Stuttgart University, (a) loading history, (b) creep deformation.

creep tests by Van Paepegem et al. [16]. The hybrid UHMWPE pads perform better elastic properties and dimensional stability through the reinforcing carbon fibre/epoxy ring (Fig. 7b).

4.4. Influence of loading geometry and lubricated interface

Fig. 8 shows test results from Stuttgart University for creep and recovery of unlubricated and lubricated UHMWPE pads. Pads are loaded against a flat counterface without a reinforcing carbon fibre/epoxy ring for stabilisation of the top surface and zero clearance. High static deformation and creep is observed compared to the composite ring reinforced UHMWPE pads (Fig. 5), with a maximum axial indentation of 0.70 mm ($\epsilon = 0.041$) for unlubricated contact and 0.81 mm ($\epsilon = 0.047$) for lubricated contact after 144 h creep at 50 MPa. Under lubrication, the immediate static deformation is not influenced, but creep becomes significantly higher.

5. Parametric study by two-dimensional simulation

A preliminary 2-dimensional finite element model is used for calculation of stresses and deformation on a constrained bearing element, where the load is applied along the Z-axis through a flat counterface and the X-axis indi-

cates the radial direction (see Fig. 1). A single bearing element is modelled with homogeneous elastic properties (the reinforcing carbon ring will be modelled in Section 6), mainly considering the stability at the free top surface and the influence of the fixation method. The radial deformation and stresses at the top surface are important for hybrid UHMWPE pads as it governs extrusion or cold-flow of the polymer lip, while the accumulation of stresses in the weak top layer is detrimental for polyester/polyester pads.

For practical design, the effect of 1 mm reversible axial compression on a single bearing element should be verified during initial contact. A large variation in radii between both curved parts however affects the sliding behaviour of the entire ball-joint. According to the experimental stress-strain characteristics under steady-state (i.e. multiple loading), an additional axial compression of 1 mm corresponds to 30 MPa additional stress, leading to possible overload on a single bearing element. This limit is based on the following:

- In situ measurements of the convex steel geometry (radius 5000 mm) reveal a maximum radial tolerance of 0.72 mm (safety factor 1.50), with (i) either a positive deviation causing locally an higher compression of the bearing element and consequently a higher stress on the element or (ii) a negative deviation causing the polymer bearing element to loose contact with the counterface and a consequent overload on a neighbouring element.
- It has been demonstrated that the clearance between the bearing element and the sample holder influences the deformability [14]. Due to production tolerances on both pad and hole diameters, the worst case of negative tolerated pad (diameter 249.37 mm) into a positive tolerated sample holder causes a 0.25 mm (safety factor 1.50) compression.

The 0.72 mm and 0.25 mm supplementary compressions result in approximately 1 mm relative variation in height between two bearing elements.

It seems mainly under low loads (10–50 MPa) that the pad geometry affects the deformation behaviour. Under higher loads, the constraining action of the steel sample holder determines the bulk modulus and ensures stability with representative creep (Fig. 6d). The deformation under 10, 30 and 50 MPa will therefore be detailed, both after *short-term* (i.e. immediate or ‘elastic’ deformation) and *long-term* (i.e. ‘plastic deformation’ or creep) loading, as a function of the following parameters:

- The pad geometry is varied with thicknesses $t = 17, 34, 51$ mm (a constant 3 mm free top surface above the sample holder is applied) and different pad diameters $D = 150, 225$ and 300 mm.
- The Young’s modulus E of the pad material is varied between 750, 1000 and 3000 MPa.

- Three fixation methods of the pads are considered, either fitting in the steel sample holder with given tolerances and no rubber O-ring for axial fixation (Type I), either with grooves in the polymer part (radius 3 mm) containing a rubber O-ring (Type II), either with a groove in the steel holder that allows for additional fixation of the polymer part by plastic flow (Type III). The latter protects a bearing element against tilting under gravity forces and asymmetric loading.

A stress–strain relation from finite element calculations on a Type I pad is given in Fig. 9 for short-term and long-term deformation under low load, indicating the effect of loading time and Young's modulus.

5.1. Short-time loading (static deformation)

Under short-term loading, some calculations for axial compression, radial expansion and effective stress are given in Figs. 10 and 11 under 30 or 50 MPa normal load with different fixations. A complex stress situation occurs in the polymer bulk, with the effective stress attaining 10 MPa under 30 MPa normal load or 18 MPa under 50 MPa normal load. The polymer bulk thus acts under elastic conditions, as the effective stress is lower than estimated from the applied normal load. Through a perfect fitting (zero tolerance) between the pad diameter and the steel holder, the constraining action implies a hydrostatic stress condition. It is seen that this state of stress most likely acts near the walls, where the effective stress is lower than in the polymer bulk for a Type I pad. Stress concentrations near the grooves for a Type II pad however indicate that the yield strength is locally exceeded under 30–50 MPa loading. From the calculated effective stress on a Type I pad under 50 MPa normal load, it reveals that the yield strength is only exceeded at the top surface, which is not constrained by the sample holder. The effective stress

attains locally 32 MPa and this explains the deformation experienced for polyester/polyester pads or cold-flow in the UHMWPE polymer lip (see Section 5.2), with a simulated lateral displacement of 0.18 mm. Under 30 MPa, a radial displacement at the free top surface of only 0.08 mm was calculated. Covering of the carbon fibre/epoxy reinforcing ring by the polymer lip was even observed during stepwise loading without long-term plastic deformation of the polymer bulk: the initial clearance between the polymer pad and the sample holder was maintained while the top surface was plastically deformed. In case of a totally constrained Type II pad not allowing for lateral displacement at the top surface, the effective stress distribution at the top edge almost equals the bulk situation (10 MPa).

The short-time axial compression of a bearing element is summarised in Fig. 12a and b as a function of the pad geometry and fixation method (intermediate Young's modulus $E = 1000$ MPa). No difference in vertical indentation is calculated depending on the pad diameter, while the total axial compression depends on the pad thickness: a higher thickness causes higher compression. The diameter has no influence on the short-term axial compression because the influence of creep and lateral displacement is constrained by the steel walls and not considered during short loading times. Plastic deformation may occur only at the edges of the free top surface, although it does not influence the global elastic behaviour: the slope of the calculated curves are linear, representing a global elastic and reversible deformation in the polymer bulk. Due to this elastic behaviour under short-time loading, also no difference in axial indentation depending on the fixation method is shown.

5.2. Long-time loading (creep deformation)

For long-time deformation, creep results in extrusion at the top surface and plasticity near the fixation grooves.

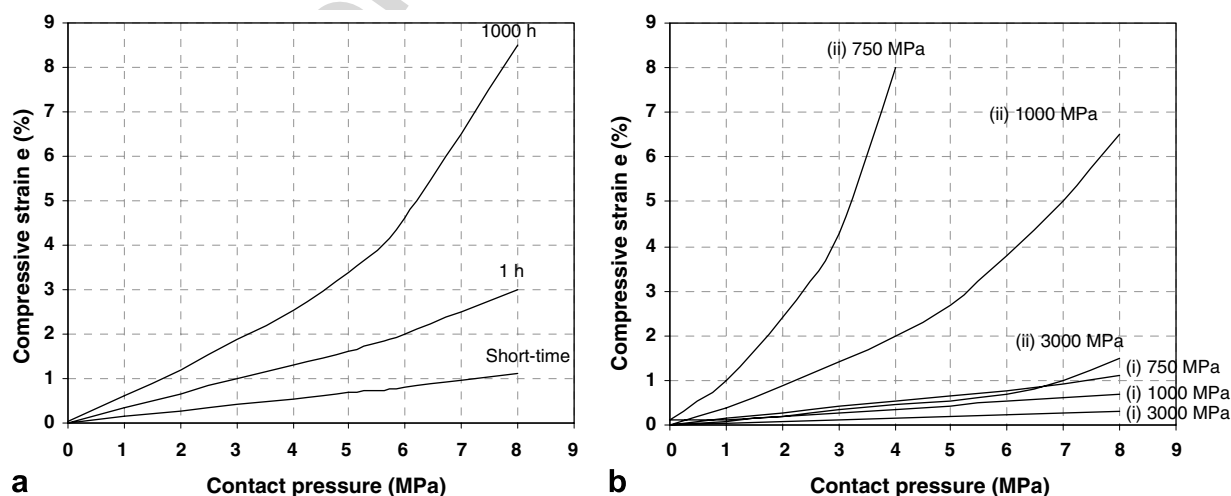


Fig. 9. Calculated stress–strain characteristics under low load from 2-dimensional finite element analysis for a Type I pad, (a) influence of loading time, (b) influence of Young's modulus E (MPa) for (i) short-time and (ii) 1000 h.

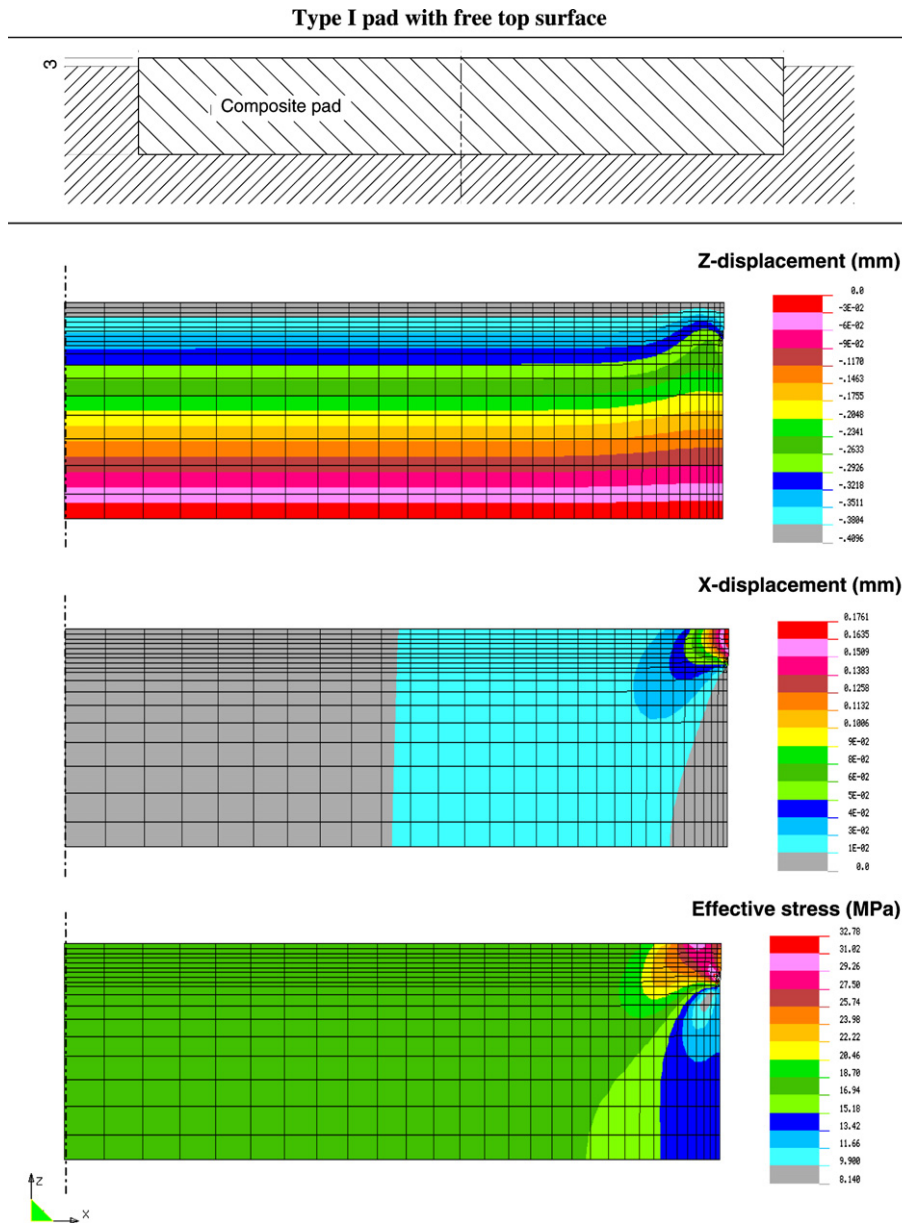


Fig. 10. Finite element simulation of stress and deformation during short-term loading under $p = 50$ MPa (Type I pad), Solico BV.

These effects are shown in Fig. 13 with simulations for a polymer with intermediate Young's modulus $E = 1000$ MPa. The creep is also influenced by dynamic sliding forces, shear stresses and eccentric loads, however not included in this static-load simulation. This was only experimentally verified and as mainly the carbon fibre/epoxy ring is radial stressed, the effect of friction induced shear stresses on dimensional stability is further simulated in a 3-dimensional model.

- Deformation at the top polymer surface is simulated as viscous polymer flow between the carbon fibre/epoxy ring and counterface, resulting in an equivalent extrusion through a small 'die' geometry. Therefore, the extrusion rate V is estimated from the relation proposed

by Michaeli et al. [21] relating to polymer extrusion: $\Delta p/L = 12\eta V/(BH^3)$, with a pressure Δp acting on the pad and the dimensions L , B and H determined by the geometry of the convex counterface and the polymer lip. Applying a constant normal load on the polymer pad, the extrusion rate diminishes with loading time as the extrusion length L increases, the height H decreases and the local pressure Δp decreases through an increase in contact area. The deformation of the top polymer surface, expressed as the extrusion length L is plotted in Fig. 13a as a function of loading time for different 'die' geometries H and normal loads (pad geometry: thickness $t = 34$ mm, diameter 225 mm). The situation of a lubricated contact (friction $\mu < 0.05$) is simulated, while it was also verified that for unlubricated sliding

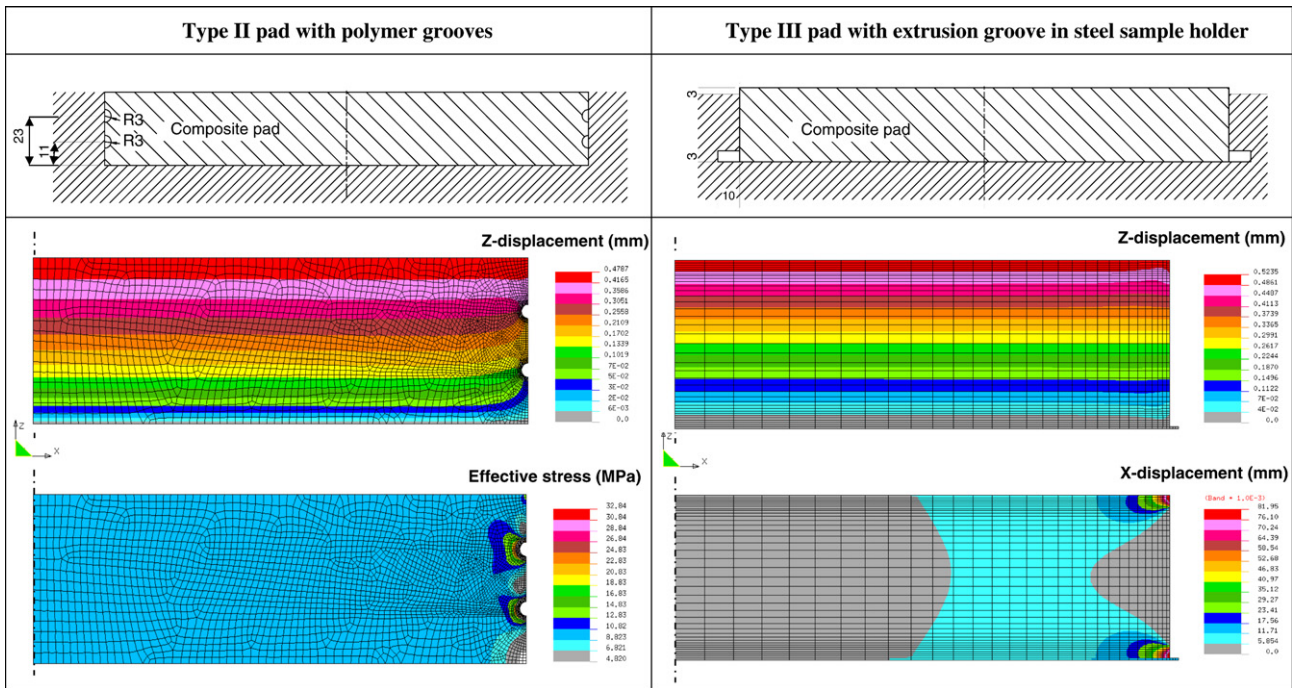


Fig. 11. Finite element analysis of stresses and deformation for different types of fixation during short-time loading under $p = 30$ MPa (Type II and Type III pads), Solico BV.

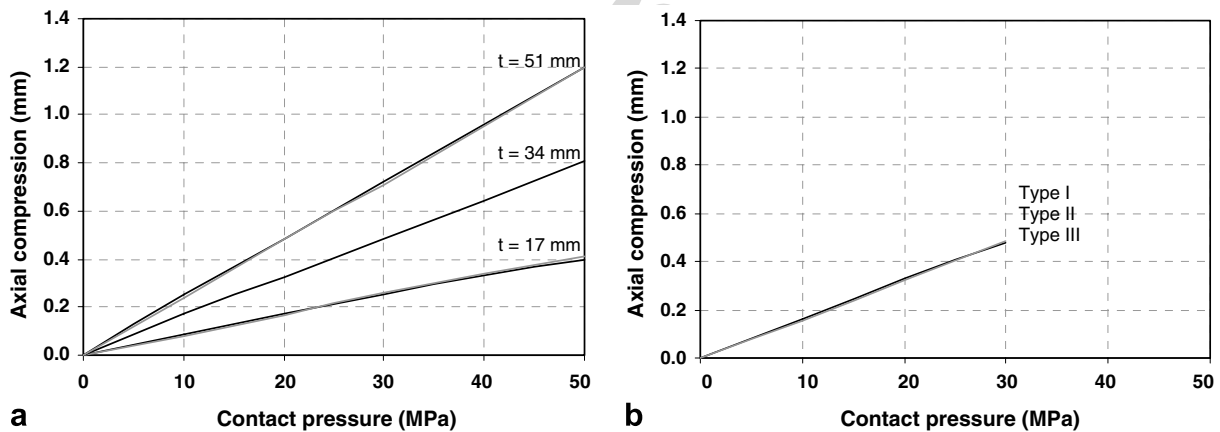


Fig. 12. Calculated short-time deformation for bearing elements, (a) influence of disc geometry for different thickness t : coinciding for pad diameters $D = 150$ mm, 225 mm and 300 mm, (b) influence of fixation method: coinciding for Type I, Type II and Type III pads.

(friction $\mu = 0.10\text{--}0.15$) the extrusion rate is lower, equalling calculations with the semi-thickness of the real gap. Corresponding to the protection of the carbon fibre/epoxy ring by permanent deformation of the polymer lip above, it is verified that the deformation of the top surface is sufficient for covering even under low loads and that the creep becomes relatively stable due to a decreasing extrusion rate. For polyester/polyester pads, it is shown both by experiments and finite element calculations that deformation at the top surface is too high, not being further considered.

- The stability of fixation grooves is also simulated by polymer extrusion through a gap with appropriate geometry. The dimensional change of the polymer groove radii (Type II) or the polymer extrusion length

into the bottom steel holder groove (Type III) is plotted in Fig. 13b and c for different normal loads as a function of the loading time. Under a given normal load, the deformation of polymer grooves is relatively faster compared to the extrusion into a groove of the sample holder, due to higher stress concentrations in the first case (see also Fig. 11). After recovery under 50 MPa loading, the deformation at the groove causes 0.50 mm non-reversible axial compression for the Type II pads and 0.56 mm for the Type III pads. The higher deformation in the latter case occurs after longer loading times.

From the assumptions above, the axial compression of a bearing element consists of a short-term (elastic) and a long-term component (creep), where mainly the latter is

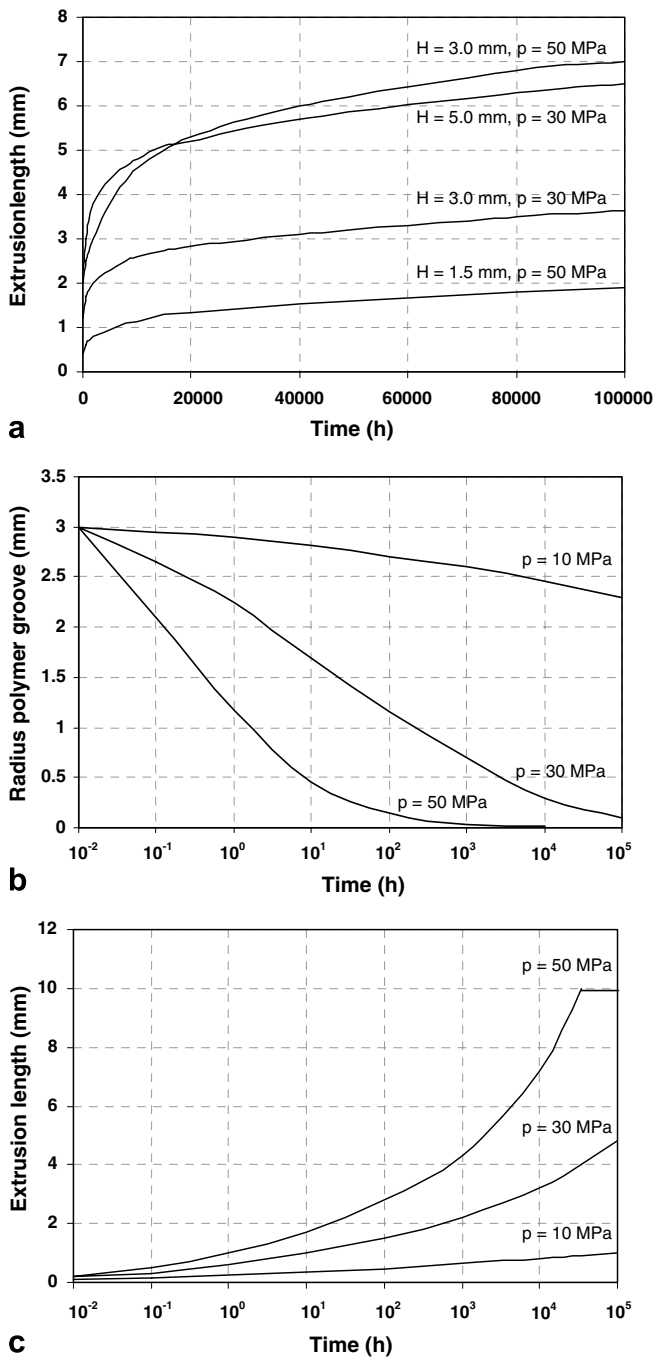


Fig. 13. Calculated long-term deformation for different pad types, (a) Type I: extrusion at the polymer top surface, (b) Type II: plastic flow at fixation grooves in the polymer, (c) Type III: extrusion in the fixation grooves of the steel sample holder.

influenced by a certain type of pad geometry. For each fixation method, the axial compression during 10 years (87,600 h) loading and recovery is simulated in Fig. 14. It reveals that the experimental curves are a combination of the models for Type I and Type II pads. The total creep however depends on the input of elasticity modulus and pad geometry (diameter D and thickness t), and the variations in axial compression for different Young's moduli is presented in Fig. 15, with e.g. lower stiffness causing higher

indentation over 10^5 h loading compared to higher stiffness. Under 50 MPa, only 6 h are simulated as a different creep regime is attained where the axial compression is stabilized through initial deformation and constraining action of the steel sample holder.

Hybrid UHMWPE pads are effectively mounted with a groove and rubber O-ring. As it possibly causes high stress concentrations, it is not incorporated into the carbon fibre/epoxy ring. It was demonstrated that high radial-axial shear stresses are detrimental for the performance of the composite ring [22]. Therefore, the composite ring does not cover the entire height of the polymer pad and a polymer protrusion near the bottom allows for a polymer groove with diameter 6 mm containing an O-ring with diameter 5.7 mm. It provides good dimensional stability and easy manual installation. The final bearing capacity exceeds 400 MPa contact pressures without local damage and good relaxation properties of the rubber O-ring after cyclic loading. The axial constraining capacity by friction between EPDM-rubber and the steel wall was also verified by a full-scale pull out test. Alternative positioning methods either based on friction of the polymer bearing element with the bottom plate of the steel holder or fixation with a bolt embedded in the centre of the pad have failed.

6. Local design analysis by three-dimensional simulation

A 3-dimensional finite element model (Fig. 16) simulates the convex counterface and action of the reinforcing carbon fibre/epoxy ring, which is considered as a load transferring element between the central UHMWPE part and the steel holder. A normal load is applied in the centre of the polymer pad parallel to the Z-axis (axial direction) with a counterface radius 5000 mm. The effect of friction is additionally simulated by applying a shear force in X direction. Nodes on the bottom of the holder are vertically fixed and horizontally free, assuming that no forces are transmitted. On the radial edges, variable contact elements are used for the contact between the carbon fibre/epoxy ring and the steel holder. The steel part is modelled as pure elastic material. Also the polymer lip on top of the ring is modelled as purely elastic (no visco-elastic properties or plastic deformation) in order to avoid extrusion. The build-up of a hydrostatic pressure under loading is simulated by a gradual decrease of the polyethylene bulk modulus in the extrusion gap.

6.1. Influence of counterface geometry: contact model

The convex counterface causes an inhomogeneous distribution of the contact pressure over the polymer surface. Hertzian contact theories [23] however cannot be applied as it assumes an infinite small and continuous contact surface in contrast to present situation of a faceted convex surface in contact with multiple bearing elements. The evolution of the contact area between ball counterface and UHMWPE pads with a carbon/epoxy reinforcing ring dur-

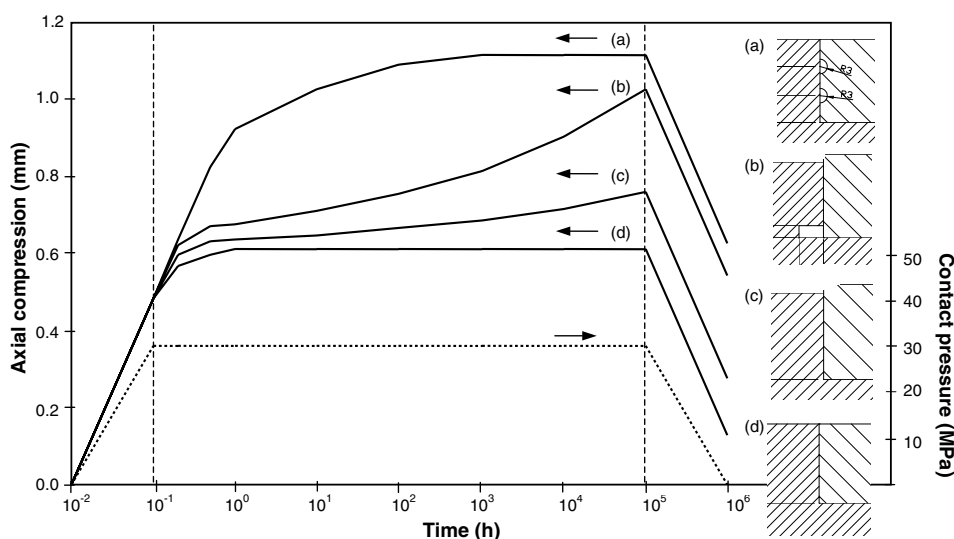


Fig. 14. Model for long-term deformation of constrained bearing elements with different fixation methods under $p = 30$ MPa (dotted line = contact pressure, full line = deformation), Solico BV.

ing short-time loading is therefore modelled in Fig. 17 in the loading range between 0 and 50 MPa.

The contact radius between the counterface and the polymer surface is plotted in Fig. 17a against the apparent contact pressure. The latter is calculated on the nominal pad diameter, corresponding to an average contact pressure on the bottom of the sample holder. The contact starts from a point contact and mainly increases under elastic deformation, i.e. for contact pressures lower than 20 MPa. In this load range, also a complex stress–strain characteristic was experienced in parallel to the variation in contact geometry (Fig. 3). When the convex counterface is not in contact with the full bearing area, higher contact pressures manifest locally. The apparent contact pressure is then proportional to the applied normal load rather than to the normal contact pressure. Above 50 MPa, full contact occurs and both the apparent and real contact pressure become similar. The real contact pressure at the UHMWPE surface is plotted in Fig. 17b along the pad diameter. At 30 MPa, there is noticed a higher real contact pressure near the borders of the polymer pad implied by the reinforcing ring. This is favourable for extrusion of the polymer lip as soon as the steel counterface makes contact with the carbon fibre/epoxy ring. For lower loads, extrusion is not necessary as no contact between counterface and ring happens.

The normal stresses σ_{ZZ} over the cross-section of a hybrid UHMWPE pad are plotted in Fig. 18 for 2–50 MPa apparent contact pressures. Under low loads, the normal stress strongly varies over the pad radius attaining 12 MPa in the centre of the pad when loaded at 2 MPa. The yield strength is locally exceeded in the centre of the pad for contact pressures above 16.3 MPa, with $\sigma_{YY} = 30.5$ MPa in the centre of the pad. Under full contact at 50 MPa, the normal stress $\sigma_{YY} = 60$ MPa becomes more homogeneous. It is however important to note a posi-

tive normal stress located at the polymer lip and the carbon fibre/epoxy reinforcing ring as it influences the stable deformation and extrusion of the polymer lip. Compared to the stress distribution in Fig. 10 under 50 MPa, differences are attributed to the effect of a convex counterface.

6.2. Influence of the steel recess reinforcement: a transition in modulus at high loads

Previous static compression tests confirm, both by experiments and simulations, that plasticity is observed above 50 MPa. Deformation then allows for disappearance of the initial clearance between polymer pad and steel sample holder, assuring total constraint. The stiffness and deformation of the polymer component is then affected by a hydrostatic state of stress developing in the pad, resulting in a stiffness of approximately 5000 kN/mm for polyester/polyester as well as hybrid UHMWPE pads under 150 MPa.

For simulating the local deformations and contact pressures on a single bearing element under high loads, its stiffness should be known. The latter is however not only determined by the intrinsic material's properties, but it is also influenced by constraint of the sample holder. Therefore, an apparent-modulus or bulk modulus rather than the Young's modulus should be used, depending on the normal load relatively to the yield stress: the stiffness at low loads is determined by an apparent modulus while it turns into a bulk modulus under high loads. They should be determined from a combined experimental-numerical approach and the transition in stress–strain relation for both loading conditions is determined by the loading time and radial expansion of the polymer pad. For isotropic structures, a bulk modulus can be calculated from the Young's modulus E and Poisson coefficient ν (Formula (3)):

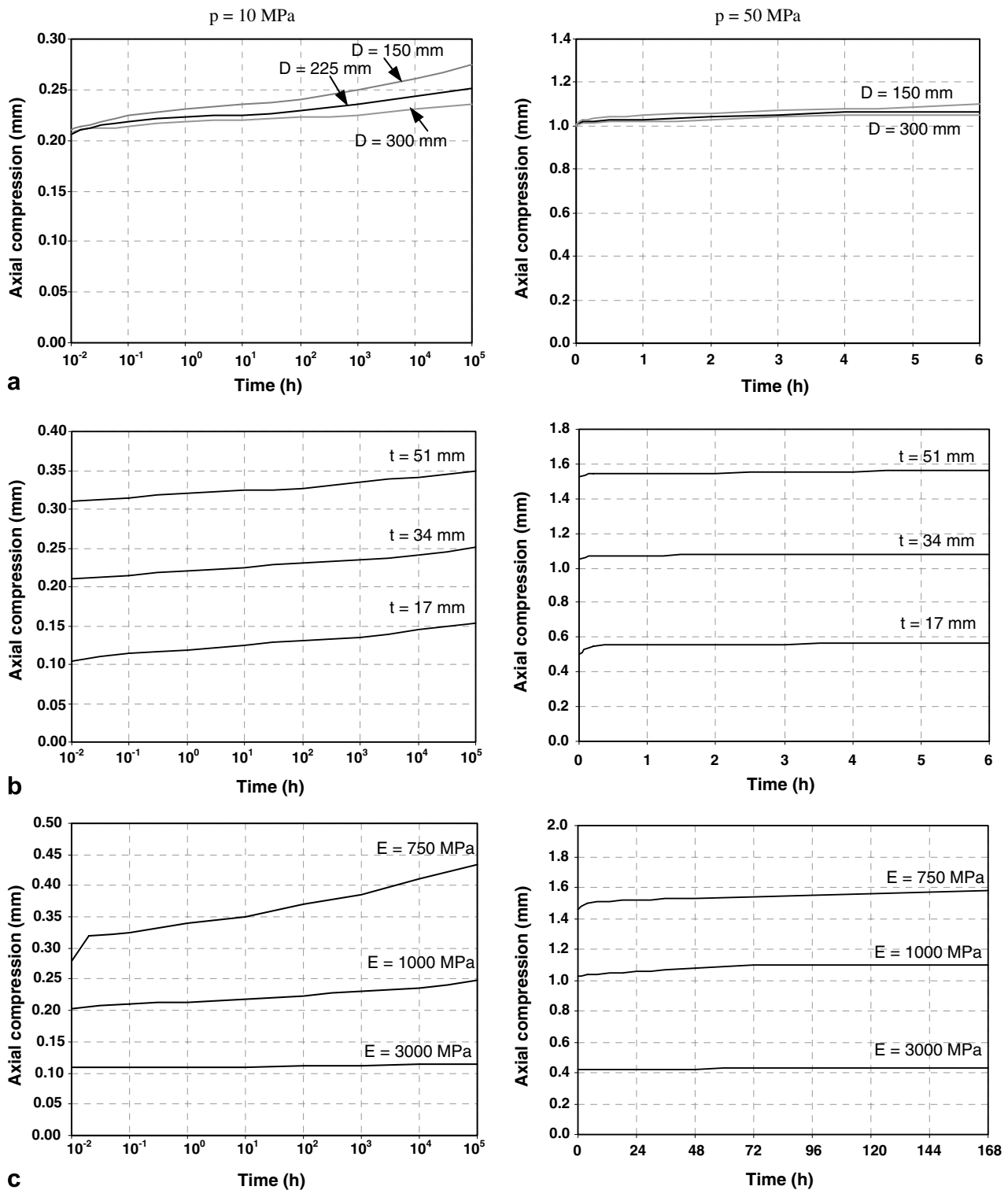


Fig. 15. Model for long-term deformation of a constrained composite bearing elements (Type I pads) under $p = 10$ MPa and $p = 50$ MPa with influence of pad geometry and material, (a) variation in pad diameter D , (b) variation in pad thickness t , (c) variation in Young's modulus.

$$\text{bulk modulus} = \frac{E}{3(1-2\nu)}. \quad (3)$$

For orthotropic structures however, no unique formula is available and a simulation should be done on different materials, as summarised in Table 3. For UHMWPE, an

experimental bulk modulus of 1600 MPa to 1850 MPa was calculated for the test geometries applied at Stuttgart University (Fig. 8) with a corresponding Poisson coefficient $\nu = 0.425$ to 0.435 . Tests at Ghent University (Fig. 3) resulted in a bulk modulus of 4200 MPa to 5000 MPa with

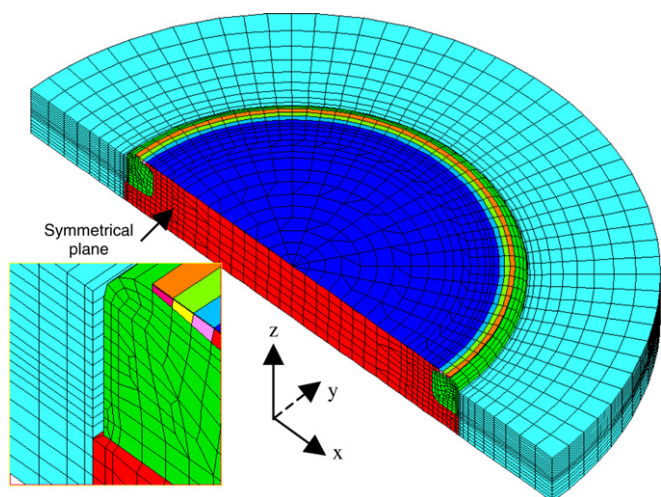


Fig. 16. 3-dimensional finite element model for a constrained hybrid UHMWPE pad, Solico BV.

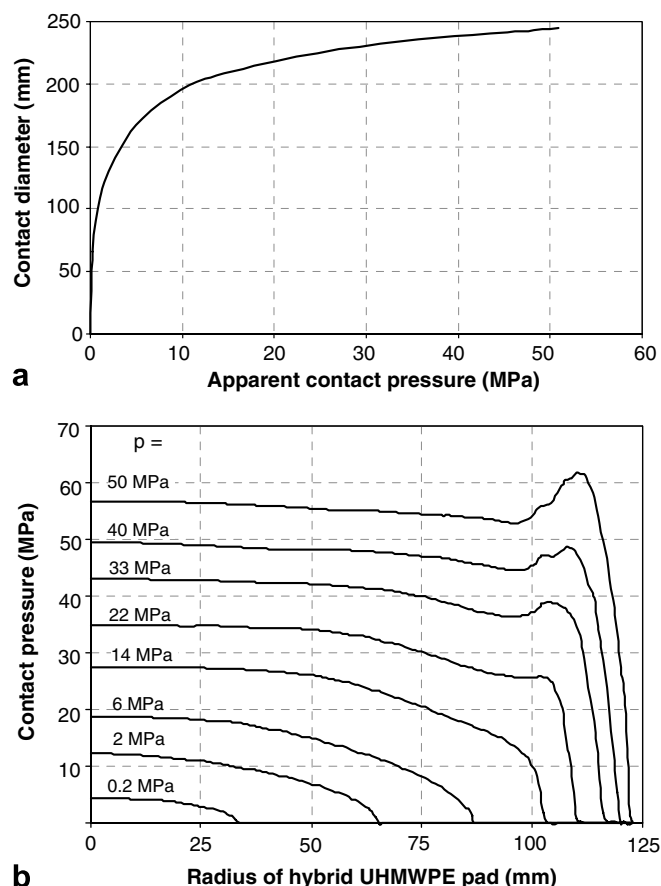


Fig. 17. Contact between a hybrid UHMWPE pad and a convex steel counterface, (a) evolution of the contact radius with applied contact pressure, (b) effective stress distribution over the pad radius for different applied normal pressures.

a Poisson coefficient $\nu = 0.473\text{--}0.476$. According to the calculated moduli, the stiffness of a constrained polymer pad is significantly higher than expected from the Young's modulus. For a bulk polymer with intermediate Young's

modulus of 1000 MPa and yield strength 20 MPa (representative for UHMWPE), the geometrical influence on the stress–strain characteristics of a constrained composite pad (zero initial clearance) is simulated in Fig. 19. Two conditions are compared: curve (a) is for a constrained polymer pad with free top surface and flat counterface (Type I pad), or curves (b, c) are for constrained polymer pads with additional carbon fibre/epoxy reinforcing ring for stabilisation of the top surface and convex counterface. A difference in stiffness under low loads is attributed to the carbon fibre/epoxy ring and a tri-linear characteristic is used for local analysis of a pad. For simulation of the strength of the global steel structure, a bi-linear function can be used. These curves agree with the observed experimental deformation of a hybrid UHMWPE polymer pad during a second loading step, i.e. with perfect fitting and zero clearance. The effectiveness of a reinforcing ring in obtaining a high bulk-modulus is demonstrated and important for the global stiffness.

6.3. Dimensional stability

For the hybrid UHMWPE pad, an optimised flexibility is required with ability for local deformation under imperfect geometrical tolerances on the convex counterface, while too high pad deformation possibly leads to direct contact between the convex and concave sliding surfaces.

As the polymer elements are loaded above their yield strength, the deformation should be stabilised by a reinforcing carbon fibre/epoxy ring. Under high load conditions and due to a hydrostatic stress component, this implies a complex stress distribution in the reinforcing carbon fibre/epoxy ring. In the present paper, the dimensional stability in terms of radial displacement will be calculated. Not only a static normal load, but also a shear load on the top surface should therefore be considered. Simulations are done under different normal loads (axial load F_z) and appropriate coefficients of friction (shear load F_x) as summarized in Table 4. The latter design values were determined from large-scale sliding experiments with a safety factor of 1.25 on frictional induced stresses.

The X-displacement of the carbon fibre/epoxy ring is shown in Fig. 20. There is noticed a smaller radial deformation of the carbon fibre/epoxy ring for higher loads, attributed to contact with the wall of the steel sample holder: it varies from maximum 1.31 mm under 30 MPa to 1.22 mm under 90 MPa and 0.94 mm under 163 MPa. Also the deformation becomes more symmetrically distributed over the ring under high loads. The locations with high radial deformation correspond to the regions with high tensile stresses σ_{YY} along the fibre direction [22]. As shown on the cross-sectional cut, the coefficient of friction plays an important role on the radial deformation: under maximum loading, the maximum radial deformation over the ring thickness in case of zero friction is lower compared to the simulations with design friction coefficients.

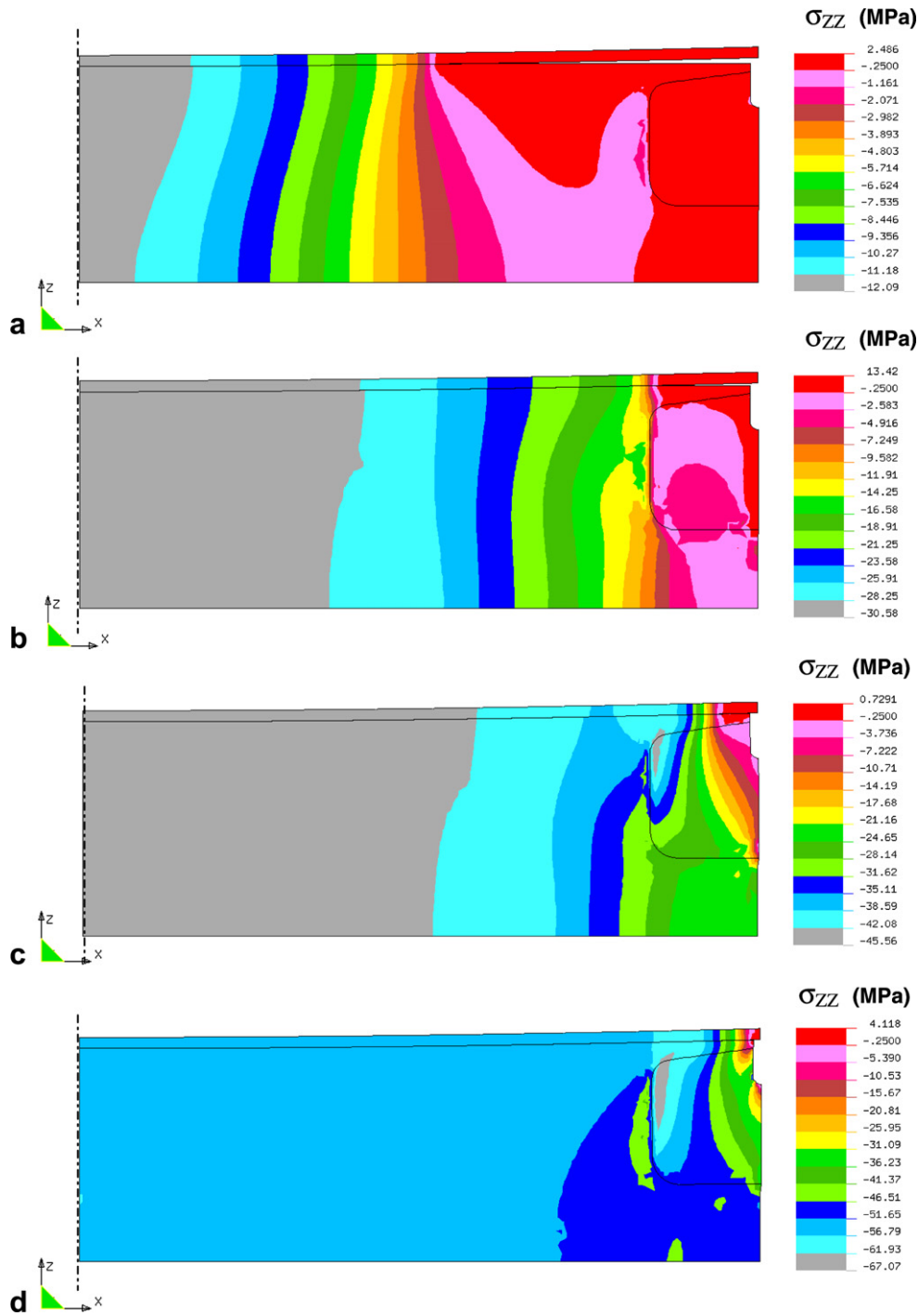


Fig. 18. Distribution of normal stresses σ_{ZZ} with evolution of the contact between a convex steel counterface and hybrid UHMWPE pad under low loads (Solico BV), (a) 100 kN or 2 MPa, (b) 800 kN or 16.3 MPa, (c) 1700 kN or 34.6 MPa, (d) 2500 kN or 50.1 MPa.

Table 3
Calculation of bulk-moduli and apparent moduli for different materials under constrained conditions (Type I pads)

	EPDM rubber	PUR	PTFE	UHMWPE	Polyester/polyester
Young's modulus (MPa)	0.92	1	600–800	750–1000	3000–3200
Poisson coefficient	0.50	0.25	0.40	0.40	0.12
Apparent modulus (MPa)	1000	0.67	1600	2100	5500
Bulk modulus (MPa)	1000	0.67	1250	1650	3800

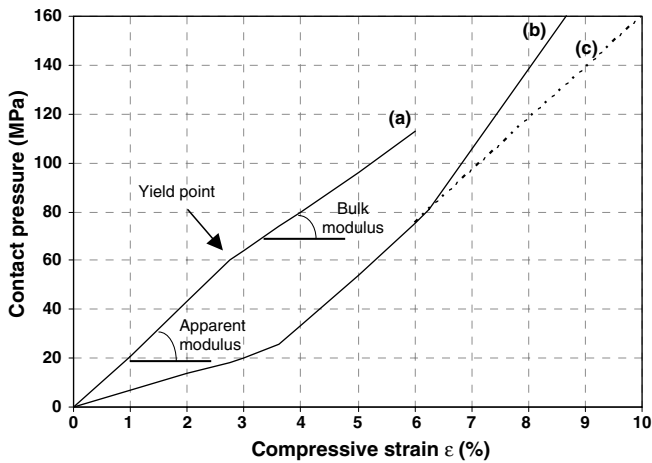


Fig. 19. Transition from apparent modulus to bulk modulus for constrained bearing elements depending on the loading geometry, (a) Type I pad with free top surface for intermediate Young's modulus $E = 1000$ MPa, (b) hybrid UHMWPE pad with reinforcing carbon fibre/epoxy ring (local analysis), (c) hybrid UHMWPE pad with reinforcing carbon fibre/epoxy ring (global analysis).

Table 4
Loading histories for full-scale finite element calculations

Loading history	Horizontal shear stress at UHMWPE surface		Finite element model	
	Effective stress (MPa)	Design stress (MPa)	Axial F_z (kN)	Shear F_x (kN)
30 MPa + $\mu = 0.21$	5.1	6.3	–1473	309
90 MPa + $\mu = 0.09$	6.3	8.1	–4418	398
163 MPa + $\mu = 0.0625$	7.5	10.2	–8000	500
163 MPa + $\mu = 0.00$	0	0	–8000	0

7. Verification of local strength

7.1. Static and dynamic strength of hybrid polymer pads

In the final ball-joint concept, failure of the bearing elements possibly occurs either by static or dynamic overload. The sliding tests after design modifications did not reveal any damage in combination with the applied normal loads, showing that both normal and shear stresses are below the bearing element capacity. Due to limitations on the available large-scale test equipment, sliding tests were only performed with a flat counterface and the effect of a convex radius should be verified by simulation.

During initial loading, the shear stresses are concentrated on a small contact area and cause a non-uniform stress distribution for a hypothetical 30 MPa apparent contact pressure (i.e. $F_z = 1473$ kN acting on a 250 mm bearing diameter). It is concluded that the strong decrease in friction coefficient for high contact pressures is more important than the decrease in contact area and therefore safe design based on experimental tests is ensured.

- Assuming a uniform contact pressure with a design friction coefficient $\mu = 0.21$ as experimentally determined, the induced shear stress τ_x equals 0.21×30 MPa =

5.1 MPa acting on the full 250 mm pad diameter. This stress corresponds to a load $F_x = 250 \text{ mm} \times 5.1 \text{ MPa} = 250$ kN.

- Assuming a non-uniform contact pressure, it was shown in Fig. 17 that the bearing element is in contact with the counterface over a diameter of 216.5 mm with an average contact pressure of 40 MPa and corresponding friction coefficient $\mu = 0.133$. The shear stress τ_x is 0.133×40 MPa = 5.3 MPa as determined by interpolation. It is then verified that the effective normal load $F_x = 216.5 \text{ mm} \times 40 \text{ MPa} = 1473$ kN does not exceed the bearing capacity and the load $F_x = 216.5 \times 5.3$ MPa = 195 kN is lower than the 250 kN under uniform contact pressure.

During steady-state loading, contact is made over the full bearing area and it can be demonstrated that a non-uniform distribution of the contact pressure does not affect the load F_x , assuming that the shear stress is linear to the apparent contact pressure: the shear stress τ_x equals respectively 5.1 MPa, 6.3 MPa and 7.5 MPa under 30 MPa, 90 MPa and 150 MPa apparent contact pressure.

7.2. Strength of the constraining steel walls

Stresses are transferred from the hybrid UHMWPE bearing element into the walls and bottom plate of the sample holder. The strength of the underlying concave structure of the ball-joint needs to be detailed and was analysed in parallel to an analysis of the global steel structure, resulting in a maximum tolerable depth of the holes of 50 mm (the effective chosen depth is $h_{\text{hole}} = 32$ mm). Considering the polymer as a 'liquid' under yielding conditions or hydrostatic pressure, it is not able to transfer horizontal shear stresses. It is the carbon fibre/epoxy ring that is loaded and transfers the loads towards the walls of the sample holder over an active height $h_{\text{eff,ring}} = 18.5$ mm that is in contact with the steel wall and width $b_{\text{ring}} = 20$ mm. The tensile and radial stress distributions are used for estimating the steel capacity under maximum contact pressure $p = 50$ MPa and maximum friction coefficient $\mu = 0.25$. As radial deformation is restricted under high loads, the sample holder can be considered as an equivalent pressure vessel with a pad diameter $D_{\text{pad}} = 250$ mm, with stresses.

7.2.1. Stress-transfer under pure hydrostatic load at $p = 150$ MPa

The average tensile force T in the carbon fibre/epoxy ring is calculated according to Formula (4). The resultant horizontal force Q acting in the centre of the pad is calculated from Formula (5):

$$T = \frac{1}{2}(D_{\text{pad}} - 2b_{\text{ring}})h_{\text{eff,ring}}p \quad (4)$$

$$Q = ph_{\text{hole}}D_{\text{pad}} - 2T \quad (5)$$

resulting in $T = 291$ kN and $Q = 618$ kN. For an active load transferring cross-section of the carbon/fibre epoxy

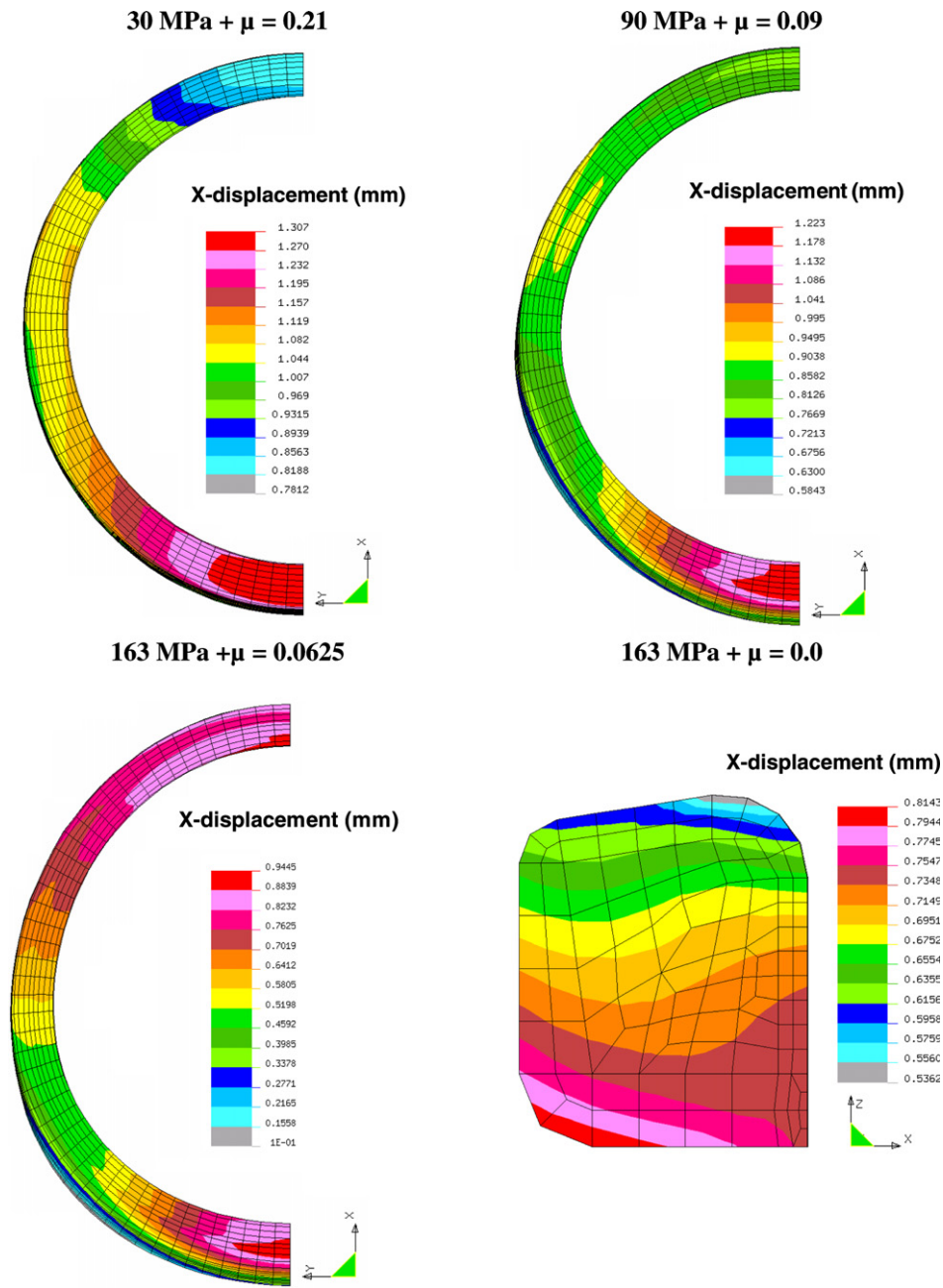


Fig. 20. Calculated radial deformation of the carbon fibre/epoxy reinforcing ring in a hybrid UHMWPE pad, Solico BV.

ring $b_{\text{ring}} \times h_{\text{eff,ring}} = 370 \text{ mm}^2$, the calculated average tensile stress σ_{YY} equals $T/(b_{\text{ring}} \times h_{\text{eff,ring}}) = 786 \text{ MPa}$ (this corresponds to an effective simulated σ_{YY} for an overload $p = 163 \text{ MPa}$). Assuming the polymer pad under hydrostatic pressure and the steel wall acting as a pressure vessel is thus a good approximation.

7.2.2. Stress-transfer under maximum frictional load (shear stress)

The horizontal friction force F transferred by the carbon fibre/epoxy ring with surface area A_{ring} is calculated from Formula (6) and added to the resultant horizontal force Q , it equals the total transmitted horizontal force on the

steel wall H given by Formula (7). The momentum M on the steel wall is calculated from Formula (8).

$$F = \mu p A_{\text{ring}} = \mu p \pi (D_{\text{pad}} - b_{\text{ring}}) b_{\text{ring}} \tag{6}$$

$$H = Q + F \tag{7}$$

$$M = \frac{1}{2} Q h_{\text{hole}} + F \left(h_{\text{hole}} - \frac{h_{\text{eff,ring}}}{2} \right) \tag{8}$$

resulting in $F = 542 \text{ kN}$, $H = 1160 \text{ kN}$ and $M = 22.22 \text{ kN m}$. For a minimum wall thickness $t = 60 \text{ mm}$, which follows from the distribution pattern of the bearing elements over the concave ball-joint surface, the maximum

shear stress τ_{\max} and normal stresses σ_{\max} are given by Formulae (9) and (10), respectively:

$$\tau_{\max} = \frac{3}{2} \frac{H}{D_{\text{pad}} t} \quad (9)$$

$$\sigma_{\max} = \frac{6M}{D_{\text{pad}} t^2} \quad (10)$$

resulting in $\tau_{\max} = 116$ MPa and $\sigma_{\max} = 148$ MPa as design values for maximum stresses in the steel wall. For a construction steel quality with yield strength 285 MPa, there is a safety-factor $f_{\text{normal}} = 285/148 = 1.93$ on yield failure by normal stresses and $f_{\text{shear}} = 285/(116\sqrt{3}) = 1.42$ on yield failure by shear in the smallest section. Present verification shows good local safety for redesign of the ball-joint while it considers that highest contact pressures and largest friction coincide on one constrained bearing element, being rather conservative.

8. Conclusions

The local behaviour of constrained hybrid UHMWPE pads and polyester/polyester pads under 150 MPa working conditions was evaluated by full-scale static loading and creep tests, for use as bearing elements in the Maeslant storm surge barrier (The Netherlands):

- Under *low loads* (<50 MPa), stress strain characteristics depend strongly on the pad geometry, Young's modulus and counterface geometry. The initial clearance gradually diminishes through visco-elastic deformation.
 - A simulation of *short-time* deformation shows that the axial compression increases for higher pad thickness, while changes in pad diameter have almost no influence during short-time loading as it is radially constrained. Important stresses accumulate near the polymer grooves for fixation, although they have no influence on the short-time loading characteristic. Also stress concentrations at the top surface are important for regular plastic flow of the polyethylene over the carbon fibre reinforcing ring.
 - After *long-term* loading, the extrusion length at the top surface is simulated and shows favourable covering of the carbon fibre/epoxy ring, which stabilises relatively in time by a decreasing extrusion rate. In this respect, also the increase in contact between the polyethylene pad and a convex steel counterface is simulated, showing full contact from 50 MPa on. Under creep conditions, the influence of the pad diameter becomes more distinct as simulated over 10^5 h. For reasons of low creep, the pad diameter should be chosen as large as possible: present parametric study in combination with a stable deformation resulted in the nominal pad diameter of 249 mm. Also different fixation methods of the composite pads into their holders clearly influence the creep strain, through stress concentrations near fixa-

tion grooves or extrusion into a gap in the steel sample holder. Higher axial compression (non-reversible) is then observed.

- For *high loads* (>50 MPa) there is a gradual increase in stiffness due to the constraining action of the steel sample holder: the pad is then under hydrostatic conditions, with a simulated stress situation that is complex near the constraining walls. This is simulated by a transition in modulus from an 'apparent modulus' to a 'bulk modulus' depending on the testing geometry (orthotropic structure) and reinforcing carbon fibre/epoxy ring. Deformation and moduli under fully constrained conditions are representative for different pad materials and creep rates for 90–150 MPa are identical.

For practical implementation in the ball-joint structure, the strength of the constraining steel walls is verified, considering the polymer material as a 'liquid' under hydrostatic pressure with tensile stresses in the carbon fibre/epoxy ring of 786 MPa, corresponding to finite element calculations. The latter provides good dimensional stability and strength to the hybrid UHMWPE bearing elements. Higher deformation (experimental) and extrusion (simulated) is measured in case of lubricated contact.

Acknowledgements

The authors of Ghent University express their gratitude to Solico B.V. and the Ministry of Transport, Public Works and Water Management (The Netherlands), allowing to present the test results and to be involved in the redesign of the Maeslant storm surge barrier.

References

- [1] Boyce MC, Socrate S, Llana PG. Constitutive model for the finite deformation stress-strain behaviour of poly(ethyleneterephthalate) above glass transition. *Polymer* 2000;41:2183–201.
- [2] Krempl E, Bordonaro C. A state variable model for high strength polymers. *Pol Eng Sci* 2000;35:310–6.
- [3] Hasan O, Boyce MC. A constitutive model for the nonlinear viscoelastic viscoplastic behavior of glassy polymers. *Pol Eng Sci* 2000;35:331–44.
- [4] Bardenhagen S, Stout M, Gray G. Three dimensional, finite deformation, viscoplastic constitutive models for polymeric materials. *Mech Mater* 1997;25:235–53.
- [5] Takashi A, Mori Y, Kaneko K. Tensile properties and stress relaxation of polypropylene at elevated temperatures. *Pol Eng Sci* 1997;37:81–90.
- [6] Yang E, Chen M. Modeling of large plastic deformation in crystalline polymers. *J Mech Phys Solids* 2001;49:2719–36.
- [7] Khan A, Zhang H. Finite deformation of a polymer: experiments and modeling. *Int J Plast* 2001;17:1167–88.
- [8] Van Dommelen JAW, Parks DM, Boyce MC, Brekelmans WAM, Baaijens FPT. Micromechanical modeling of the elasto-viscoplastic behaviour of semi-crystalline polymers. *J Mech Phys Solids* 2003;51:519–41.
- [9] Bergström JS, Boyce MC. Constitutive modeling of the large strain time-dependent behavior of elastomers. *J Mech Phys Solids* 1998;46:931–54.

- [10] Malinin NN, Khadjinsky GM. Theory of creep with anisotropic hardening. *Int J Mech Sc* 1972;14:235–46.
- [11] Krempf E, Ho K. An overstress model for solid polymer deformation behaviour applied to Nylon 66. *ASTM STP* 2000;1357:118–37.
- [12] Colak O. Modeling deformation behaviour of polymers with viscoplasticity theory based in overstress. *Int J Plast* 2005;21:145–60.
- [13] Samyn P, Van Schepdael L, Leendertz JS, Gerber A, Van Paepegem W, De Baets P, et al. Large-scale friction and wear tests on a hybrid UHMWPE-pad/Primer Coating combination used as bearing element in an extremely high-loaded ball-joint. *Tribol Int* 2006;39(8):796–811.
- [14] Samyn P, Van Schepdael L, Leendertz JS, Van Paepegem W, De Baets P, Degrieck J. Deformation of reinforced polymer bearing elements on full-scale compressive strength and creep tests under yielding conditions. *Polymer Test* 2006;25(2):230–45.
- [15] Leendertz JS, Van Schepdael L, Van Paepegem W, Samyn P, De Baets P, Degrieck J. Modification of the ball bearing of the storm surge barrier near Rotterdam (NL). *Stahlbau* 2006;75(1):45–54.
- [16] Van Paepegem W, Van Schepdael L, Degrieck J, Samyn P, De Baets P, Suister E, et al. Characterization of composites for use in the ball-joints of the Maeslant storm surge barrier. *Polym Composite* [in press].
- [17] Busak and Shamban, [Composiet Materialen] (in Dutch), *Composite Materials* (1998).
- [18] Ticona GmbH. Ultra high molecular weight polyethylene: Product Catalogue GUR; 2002.
- [19] Kurtz SM, Pruitt L, Jewett CW, Crawford RP, Crane DJ, Edidin AA. The yielding, plastic flow and fracture of UHMWPE used in total joint replacements. *Biomaterials* 1998;19:1989–2003.
- [20] Scott DW, Zureick AH. Compression creep of pultruded e-glass/vinylester composite. *Composites Science Technol* 1998;58:1361–9.
- [21] Michaeli W. Extrusion dies for plastics and rubber. New York: Carl Hanser Verlag; 2003, ISBN 3-446-22561-7.
- [22] Samyn P, Van Schepdael L, Leendertz JS, Gerber A, Van Paepegem W, De Baets P, et al. Fracture assessment of carbon fibre/epoxy reinforcing rings through a combination of full-scale testing, small-scale testing and stress modeling. *Appl Compos Mater* 2006;13(2):570–85.
- [23] Hamrock BJ, Jacobson BO, Schmid SR. *Fundamentals of machine elements*. Wcb/Mcgraw-Hill; 1999.

Author's personal